# UNCLASSIFIED

## AD 433193

# DEFENSE DOCUMENTATION CENTER

FOR

## SCIENTIFIC AND TECHNICAL INFORMATION

CAMERON STATION, ALEXANDRIA, VIRGINIA

# UNCLASSIFIED

64-10

# ULTRASONIC WAVE PROPAGATION AND INTERACTION IN SOLID MATERIALS

TECHNICAL DOCUMENTARY REPORT NO. ML-TDR-64-21, Pt. I

March 1964

Air Force Materials Laboratory
Research and Technology Division
Air Force Systems Command
Wright-Patterson Air Force Base, Ohio

Project No. 7360; Task No. 736002

# NOTICES

When Government drawings, specifications, or other data are used for any purpose other than in connection with a definitely related Government procurement operation, the United States Government thereby incurs no responsibility nor any obligation whatsoever; and the fact that the Government may have formulated, furnished, or in any way supplied the said drawings, specifications, or other data, is not to be regarded by implication or otherwise as in any manner licensing the holder or any other person or corporation, or conveying any rights or permission to manufacture, use, or sell any patented invention that may in any way be related thereto.

Qualified requesters may obtain copies of this report from the Defense Documentation Center (DDC), (formerly ASTIA), Cameron Station, Building 5, 5010 Duke Street, Alexandria 4, Virginia.

This report has been released to the Office of Technical Services, U. S. Department of Commerce, Washington 25, D.C., for sale to the general public.

Copies of this report should not be returned to the Research and Technology Division unless return is required by security considerations, contractual obligations, or notice on a specific document.

## FOREWORD

This report was prepared by Midwest Research Institute under USAF Contract No. AF 33(657)-11006. The contract was initiated under Project No. 7360, "The Chemistry and Physics of Materials," and Task No. 736002, "Nondestructive Methods." The work was administered under the AF Materials Laboratory, Research and Technology Division, Air Force Systems Command, with Mr. Harold Kamm acting as project engineer.

The period of work covered by this report is from 1 March 1963 to 28 November 1963.

The experimental work was largely conducted by Mr. F. R. Rollins, Jr., and Mr. Paul Todd. Most of the theoretical work was performed by Mr. L. Taylor. Mr. Rollins served as project leader under the supervision of Dr. Sheldon L. Levy, Director of the Mathematics and Physics Division.

# ABSTRACT

The interaction of ultrasonic beams in solid media has been investigated from both the theoretical and experimental viewpoint. An error in the previously reported classical calculation has been corrected and relatively good qualitative agreement now exists between the classical and quantum mechanical calculations. Experiments are described which verify certain theoretical predictions concerning the magnitude of interaction and the conditions of resonance. Techniques have been devised for producing interaction in specimens of unusual shape. Furthermore, the feasibility of using interaction techniques in making a three-dimensional analysis of elastic anisotropy has been demonstrated.

This technical documentary report has been reviewed and is approved.
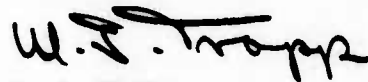
W. J. TRAPP
Chief, Strength and Dynamics Branch
Metals and Ceramics Division
Air Force Materials Laboratory

TABLE OF CONTENTS

## ILLUSTRATIONS

# I. INTRODUCTION

This report covers work performed during an investigation of ultrasonic wave propagation and interaction in solid materials. The work is essentially a continuation of an earlier contract* which was directed toward a study of ultrasonic methods for the nondestructive measurement of residual stress. In the earlier investigation certain stress-dependent aspects of ultrasonic propagation in solids were explored in the hope that a thorough understanding of these properties would facilitate the ultimate use of ultrasonics in all types of stress measurement problems including the nondestructive measurement of residual stress.

The propagation velocity of ultrasonic waves in solids varies with stress in a manner that depends on the third-order elastic constants. In addition, shear-wave velocity depends upon the angle between the polarization axis and the stress direction. These properties can combine to produce an effective rotation of the polarization axis as the shear wave travels through a stressed medium. The effect is in many respects very similar to certain photoelastic effects. Techniques for observing and utilizing the stress-dependent aspect of shear-wave propagation have been described in earlier reports.[1-3] R. T. Smith[4] has recently written an excellent review article on the use of ultrasonics in the study of stress-induced anisotropy.

During the final few months of the earlier contract a significant discovery was made relative to the experimental interaction of ultrasonic beams. The intersection of pulsed ultrasonic beams under "resonant" conditions revealed that interaction effects are indeed detectable. A theoretically predicted[5] third beam (generated at the point of intersection) was experimentally observed in a number of materials. Some experimental results have been reported in a previous report[3] and paper.[6]

The study of interaction phenomena has continued during this report period with emphasis being placed on a thorough understanding of the basic effect. A cross-check between a quantum mechanical approach and the previously derived classical results has revealed an error in the classical calculations. The corrected amplitude expressions show some extremely interesting relationships between the various interaction cases and the dependence of the interaction magnitude on third-order elastic constants. In addition, experimental effort has been directed toward a more complete understanding of

(1) sensitivity of interaction magnitude to deviations from resonant conditions, (2) correlation with theoretical predictions, and (3) techniques of introducing the ultrasonic beams into test specimens. Although much of our recent work has been of a rather basic nature, we have not overlooked possible applications of the interaction phenomenon in testing material properties. The feasibility of using interaction techniques in making a three-dimensional analysis of elastic anisotropy has in fact been demonstrated. Other areas of possible application are discussed in subsequent sections of this report.

## II. THEORY RELATED TO INTENSITY OF ULTRASONIC BEAMS GENERATED THROUGH INTERACTION

Expressions for the displacement amplitude of ultrasonic beams arising from various interaction cases were given in the Appendix of Ref. 3. These expressions were derived using the classical approach described in other reports.[2,5] During the past few months we have extended the quantum mechanical approach[3] (used previously only to calculate transition probabilities) to get amplitude expressions (see Appendices II and III), that could be compared with those obtained using the classical approach. The resultant expressions did not agree. Although exact agreement was not expected for the entire expressions, certain terms appeared much too far out of line. In attempting to run down the source of disagreement, an error was found in the classical calculations. One term had been inadvertently dropped from the defining expression for the vector $\vec{I}^{\pm}$. The correct expression is given below:

$$
\begin{aligned}
\vec{I}^{\pm} = &-\frac{1}{2}(\mu+A/4)\left\{(\vec{A}_o\cdot\vec{B}_o)(\vec{k}_2\cdot\vec{k}_2)\vec{k}_1 \pm (\vec{A}_o\cdot\vec{B}_o)(\vec{k}_1\cdot\vec{k}_1)\vec{k}_2 \right. \\
&+ (\vec{B}_o\cdot\vec{k}_1)(\vec{k}_2\cdot\vec{k}_2)\vec{A}_o \pm (\vec{A}_o\cdot\vec{k}_2)(\vec{k}_1\cdot\vec{k}_1)\vec{B}_o + 2(\vec{A}_o\cdot\vec{k}_2)(\vec{k}_1\cdot\vec{k}_2)\vec{B}_o \\
&\left. \pm 2(\vec{B}_o\cdot\vec{k}_1)(\vec{k}_1\cdot\vec{k}_2)\vec{A}_o\right\} - \frac{1}{2}(K+\mu/3+A/4+B)\left\{(\vec{A}_o\cdot\vec{B}_o)(\vec{k}_1\cdot\vec{k}_2)\vec{k}_2 \right.\\
&\left. \pm (\vec{A}_o\cdot\vec{B}_o)(\vec{k}_1\cdot\vec{k}_2)\vec{k}_1 + (\vec{B}_o\cdot\vec{k}_2)(\vec{k}_1\cdot\vec{k}_2)\vec{A}_o \pm (\vec{A}_o\cdot\vec{k}_1)(\vec{k}_1\cdot\vec{k}_2)\vec{B}_o\right\} \\
&- \frac{1}{2}(A/4+B)\left\{(\vec{A}_o\cdot\vec{k}_2)(\vec{B}_o\cdot\vec{k}_2)\vec{k}_1 \pm (\vec{A}_o\cdot\vec{k}_1)(\vec{B}_o\cdot\vec{k}_1)\vec{k}_2 + (\vec{A}_o\cdot\vec{k}_2)(\vec{B}_o\cdot\vec{k}_1)\vec{k}_2 \right.\\
&\left. \pm (\vec{A}_o\cdot\vec{k}_2)(\vec{B}_o\cdot\vec{k}_1)\vec{k}_1\right\} - \frac{1}{2}(B+2C)\left\{(\vec{A}_o\cdot\vec{k}_1)(\vec{B}_o\cdot\vec{k}_2)\vec{k}_2 \pm (\vec{A}_o\cdot\vec{k}_1)(\vec{B}_o\cdot\vec{k}_2)\vec{k}_1\right\} \\
&- \frac{1}{2}(K-\frac{2}{3}\mu+B)\left\{(\vec{A}_o\cdot\vec{k}_1)(\vec{k}_2\cdot\vec{k}_2)\vec{B}_o \pm (\vec{B}_o\cdot\vec{k}_2)(\vec{k}_1\cdot\vec{k}_1)\vec{A}_o\right\}
\end{aligned}
$$

The last term that is underlined was erroneously left out of the original calculation.[2,5] Appendix III contains the corrected classical expressions along with the expressions derived using quantum mechanical techniques. Except for the multiplying coefficient, the agreement between the expressions is very good.

One of the factors that led us to suspect the validity of the original classical calculations was the apparent lack of internal agreement between interaction cases that we considered to be somewhat equivalent. Table 1, republished from previous reports,[2,3] lists five independent cases in which interaction should occur. It is true these five cases have an element of independence, but there is also an element of equivalence. For example, if we consider the modes of all waves involved (i.e., the two primary waves as well as the resonant wave) we note that Case I and Case V are similar in that one longitudinal wave and two transverse waves are involved. Likewise, Cases II, III, and IV are similar in that one transverse wave and two longitudinal waves are involved. The similarity is even more obvious when we consider Figure 1. Looking first only at the solid lines, we see that they represent Case III of Table 1. The angle, $\phi$ , must of course satisfy the resonant condition for this interaction and the scattered wave travels in the $\bar{k}_3$ direction as defined by $(\bar{k}_1 + \bar{k}_2)$. Remembering that the angular relationship between the vectors represents the conservation of wave number and the frequency relationship is tied to the conservation of energy, it is not difficult to see that all of the interaction cases listed in Table 2 can be satisfied by interchanging the various waves in Figure 1.

If one plots the amplitude or intensity of the generated wave against the frequency ratio, $a = \omega_2/\omega_1$ , for a particular interaction case, it is often found that the generated wave amplitude goes to zero at some value of this ratio (see graphs in Appendix III). Before correcting the error in the original classical calculation, we were somewhat disturbed by the fact that the "related" interaction cases* did not exhibit zero amplitude at equivalent values of the frequency ratio. After correction, and agreement with the quantum mechanical expressions, we now find that the related cases do indeed "go to zero" at equivalent values of the frequency ratio. This can be best illustrated by referring back to Figure 1 and Table II. Let us assume that the intensity of the interaction Case III,

$$L(\omega_1) + T(\omega_2) \longrightarrow L(\omega_3) \quad ,$$

goes to zero when $a = 7/5$ , i.e., for the condition,

$$L(5) + T(7) \longrightarrow L(12) \quad .$$

---

* The related cases are: IA and VA; IB and VB; and II, III, and IV.

## TABLE 1

## INTERACTION CASES WHICH PRODUCE A SCATTERED WAVE

| Case | Primary Waves | Resonant Wave Type and Frequency | Direction of Scattered Wave | $\cos \phi$* |
|------|---------------|----------------------------------|-----------------------------|--------------|
| I | Two transverse | Longitudinal $(\omega_1+\omega_2)$ | $\hat{k}_1+\hat{k}_2$ | $c^2+\left[(c^2-1)(a^2+1)\Big/2a\right]$ |
| II | Two longitudinal | Transverse $(\omega_1-\omega_2)$ | $\hat{k}_1-\hat{k}_2$ | $1/c^2+\left[(c^2-1)(a^2+1)\Big/2ac^2\right]$ |
| III | One longitudinal and one transverse** | Longitudinal $(\omega_1+\omega_2)$ | $\hat{k}_1+\hat{k}_2$ | $c+\left[a(c^2-1)\Big/2c\right]$ |
| IV | One longitudinal and one transverse** | Longitudinal $(\omega_1-\omega_2)$ | $\hat{k}_1-\hat{k}_2$ | $c+\left[a(1-c^2)\Big/2c\right]$ |
| V | One longitudinal and one transverse** | Transverse $(\omega_1-\omega_2)$ | $\hat{k}_1-\hat{k}_2$ | $1/c+\left[(c^2-1)\Big/2ac\right]$ |

* $\phi$ is the angle between $\hat{k}_1$ and $\hat{k}_2$ at resonance.

  a is the frequency ratio $\omega_2/\omega_1$.

  c is the velocity ratio $c_t/c_\ell$.

** The frequency of the longitudinal primary wave is $\omega_1$.

4

Figure 1 - Angular Relationships Between "Related" Interaction Cases

TABLE 2

INTERACTION CASES REPRESENTED IN FIGURE 1

| Interaction Case | Resonance Angle | Direction of Primary Waves | Direction of Scattered Waves |
|---|---|---|---|
| $L(\omega_1) + T(\omega_2) \longrightarrow L(\omega_3)$ <br> Case III | $\phi_1$ | $\vec{k}_1$ and $\vec{k}_2$ | $\vec{k}_3$ |
| $L(\omega_3) + T(\omega_2) \longrightarrow L(\omega_1)$ <br> Case IV | $\phi_2$ | $\vec{k}_3$ and $\vec{k}_2$ | $\vec{k}_1$ |
| $L(\omega_1) + L(\omega_3) \longrightarrow T(\omega_2)$ <br> Case II | $\phi_3$ | $\vec{k}_1$ and $\vec{k}_3$ | $\vec{k}_2$ |

We would then expect the Case IV interaction,

$$L(12) + T(7) \longrightarrow L(5) \quad \text{with} \quad a = 7/12 \quad ,$$

and the Case II interaction,

$$L(12) + L(5) \longrightarrow T(7) \quad \text{with} \quad a = 5/12 \quad ,$$

to also go to zero. A close examination and comparison of the amplitude curves (see Appendix III) for related cases indicates that this relationship between the zeros does hold. Moreover, the entire transition probabilities between related cases have been shown to be exactly equivalent when the number of phonons of the second wave is much greater than unity.*

There is another aspect of the amplitude expressions that is very interesting. If we consider the related cases (II, III, and IV), we note that the part of the "$\delta$" term that forces the amplitude expression to zero, as the frequency ratio is varied, does not depend on the third-order elastic constants. This is particularly evident in Case II where two longitudinal waves interact and $\delta = \left[(2B+A+K+\frac{7\mu}{3})\cos\phi\right]$. The $\cos\phi$ term goes to zero when $\phi = 90°$, i.e., when the two primary longitudinal beams are perpendicular.

---

* The geometrical volume of interaction is not equivalent in related cases. Hence, the amplitude expressions in Appendix III are not exactly equivalent.

In fact, it can be easily shown that the amplitude becomes zero in all three cases, whenever the resonant conditions necessitate the two longitudinal waves being orthogonal. It should be emphasized that this condition holds true irrespective of the material in which the interaction occurs. In contrast, the amplitude expressions for the related Cases (I and V) can also go to zero (entire "$\delta$" term), as evidenced in the plotted curves, but in these cases the zero point depends on the third-order elastic constants of the material. Also in contrast, one does not find the zero point characterized by a fixed angular relationship between any of the three waves as there was in Cases II, III and IV. The shape of the curves in Appendix III emphasizes the different character of the $\delta$ term for the related Cases (I and V) or (II, III and IV). In the former cases the shape is very dependent on the material whereas in the latter cases the shape is relatively independent of the material.

Some of the other similarities and disagreements between the classical and quantum mechanical expressions should also be mentioned. In each case, $X_3$, the displacement amplitude of the third beam is proportional to the product of the primary displacement amplitudes and the common $\delta$ term. Beyond this, there is little apparent agreement between the classical and quantum expressions. It is the $\delta$ term, however, that primarily influences the shape of the amplitude curves (as shown in Appendix III) so the remaining terms that are in disagreement act as a multiplying factor that shifts the curve up or down with only a slight influence on the shape of curve. The frequency dependence is consistently different in the two approaches. There is an $\omega_1^3$ dependence in the classical case and an $\omega_1^{3/2}$ dependence in the quantum case. The classical approach leads to a $r^{-1}$ fall-off in $X_3$ whereas in the quantum case we have treated all three beams as plane waves neglecting both diffraction and dissipation.

An interesting, and fundamental, difference between the classical and quantum mechanical approaches is exhibited by the amplitude expressions for Case II. When the two primary waves are identical, classical physics requires the amplitude expressions to be independent of the labeling of the two waves. The classical and quantum mechanical amplitude expressions for Case I do indeed have this labeling independence. However, in Case II the quantum mechanical amplitude expression does not have this independence whereas the classical amplitude expression does. The reason for this is quite simple. Classically both primary waves participate equally in the interaction. Quantum mechanically one phonon splits whereas the other phonon merely acts as an "enhancer" to the interaction and is not physically transformed. Therefore, in difference frequency cases, the two primary phonons are not identical and can be differentiated between.* Mathematically this difference appears as a $(N_2+1)$ term in the transition probability where $N_2$ is the number of "enhancing" phonons. Hence as $N_2$ becomes very large with respect to unity the classical result of labeling independence is approached.

---

* This difference makes a parametric amplifier theoretically feasible.

7

### III    EXPERIMENTAL RESULTS RELATED TO
### SCATTERED WAVE INTENSITY

## A. General

During the past year, we have performed a relatively large number
of experiments related to the interaction phenomena. Most of the successful
experiments have been confined to specimens of fused silica, polycrystalline
aluminum, and polycrystalline magnesium. Unsuccessful experiments have been
attempted in polystyrene and polycrystalline iron. The two latter materials
exhibted greater attenuation than the other three and it is probably this
property that most strongly influences our ability to pick the scattered-wave
signals out of the noise.

The accurate measurement of absolute intensity of megacycle ultra-
sonic waves in solid materials is a fairly difficult problem; however, a
number of indirect techniques have been developed for this purpose. Fleury
and Alers[7] have conducted a comparative study of several such techniques
and found them to be in reasonably good agreement. Several of their tech-
niques are not adaptable to the pulsed conditions and specimen geometries re-
quired in interaction experiments. Thus far, we have restricted our attempts
to measure primary and scattered wave intensities to simple calculations
based on the equivalent circuit theory of piezoelectric transducers. Fluery
and Alers found that such calculated values deviated from more consistent
values, obtained using other techniques, by several hundred per cent. The
largest source of error in the calculated values is probably the bond between
the transducer and the test specimen. The quality and type of bond strongly
affect the mechanical power delivered to the specimen.

We have measured the intensities for many different interaction
cases. Repetition of the same experiment with different transducer bonds
indicates that reproducibility is pretty good if care is taken during the
bonding procedure. In a fairly typical case, two transverse beams of approx-
imately 1 $w/cm^2$ produced a sum-frequency longitudinal beam with an intensity
of about $10^{-6}$ $w/cm^2$. It would be desirable to compare the "experimental" in-
tensity of the generated beam with the intensity that could be calculated
from the theories of interaction. The latter calculation of course requires
knowledge of the third-order elastic constants (see expressions in Appendix
III) but unfortunately these constants are not known for the materials with
which we have been working.

8

Many of the interaction experiments discussed in this report have been performed with several thousand volts applied to the primary transducers. However, we have also performed tests to see just how low the voltage across the primary transducers could be reduced and still produce a detectable scattered wave. One such experiment was performed in fused silica by intersecting two 15 Mc shear waves to produce a 30 Mc longitudinal wave. The primary beams were produced by driving 5 Mc transducers at their third harmonic. The scattered wave signal was still easily detectable with 70 v. peak-to-peak applied to the primary transducers. These results indicate that moderate voltages applied to primary transducers can produce detectable interaction effects. The "threshold" primary voltage would have been reduced further if 15 Mc fundamental crystals were used instead of the 5 Mc transducers. The 70 v. signal mentioned above is not an uncommon voltage for delay line inputs. We would therefore expect that spurious signals could very easily arise in delay lines where "information" intersects other "information" at the angle of resonance.

## B. Relative Comparison of Primary and Scattered Beam Amplitudes

The expressions that appear in Appendix III all indicate that the scattered wave amplitude should be proportional to the product of the primary beam amplitudes. An experimental confirmation of this relationship has been obtained in several different experiments. One such experiment was performed using the interaction,

$$T(\omega_1) + T(\omega_1) \longrightarrow L(2\omega_1) \quad .$$

In this case both primary transducers were driven with the same generator. We would therefore expect the scattered wave amplitude to be proportional to the square of the primary wave amplitudes. It can be shown from piezoelectric equivalent circuit theory that when half-wave transducers are driven at resonance the displacement amplitude and voltage are linearly related. Under these circumstances, the voltage generated by the receiving (generated wave) transducer should be proportional to the square of the voltage applied to the two primary transducers. Figure 2 shows how closely this relationship was followed.

## C. Dependence on Frequency of Primary Waves

It was mentioned earlier that a discrepancy exists between the classical and quantum amplitude expressions relative to the frequency dependence.

9
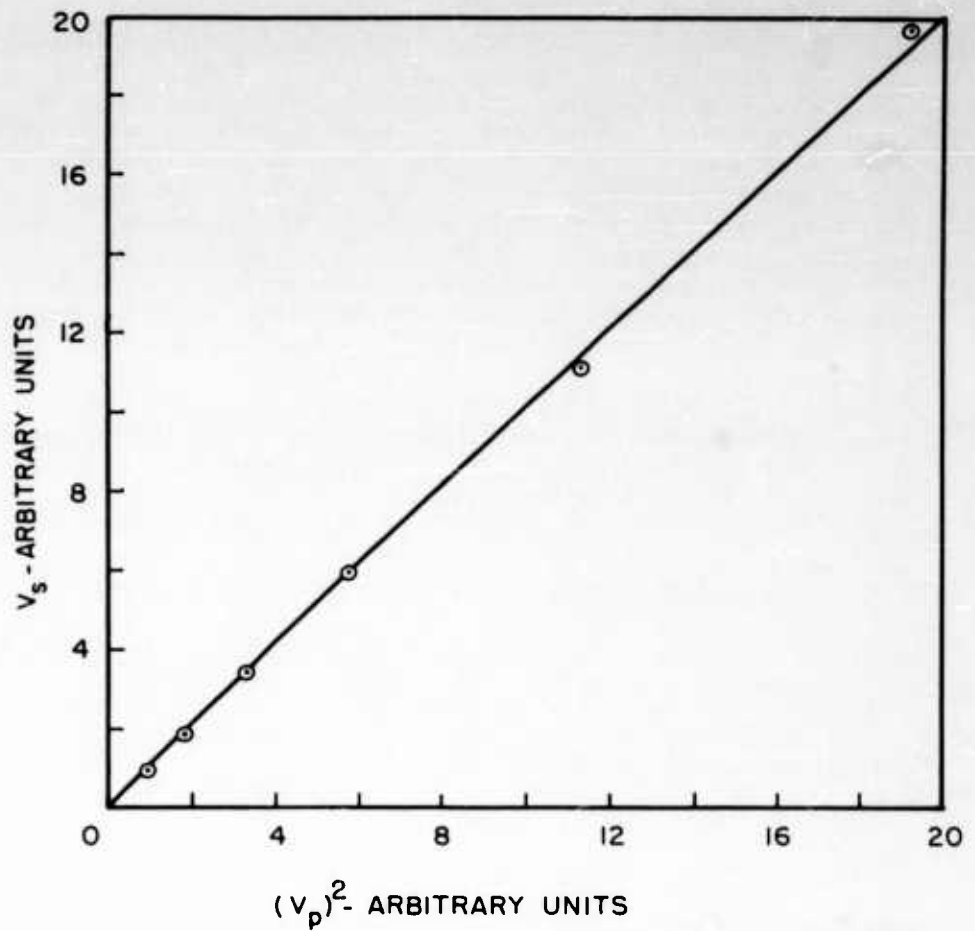
Figure 2 - Curve Showing Linear Relationship Between $(V_p)^2$
and $V_s$ where $V_p$ is the Voltage Applied
to the Two Primary Transducers and
$V_s$ is the Transducer Voltage
Produced by the Scattered Wave

The displacement amplitude of the generated beam is proportional to $\omega_1^3$ in the classical theory but it is proportional to $\omega_1^{3/2}$ in our quantum mechanical calculations (see Appendix III). It appears that the lower power on $\omega_1$ in the quantum mechanical treatment comes directly from our interpretation of the transition probability as developed in Appendix II.

Since much of the future work in phonon-phonon interactions will be performed at frequencies much higher than those used in this program, it is very important to know the exact relationship between $X_3$ and $\omega_1$. We have attempted to solve this question by comparison with experimental results but the scatter in our data was great enough to prevent any definite conclusions. A reduction in data scatter should be attainable with greater care in the bonding of transducers. In addition, study of a wider range of frequencies (over an order of magnitude) with suitable corrections for attenuation should reveal the true nature of the frequency dependence.

## D. Detection of Zero-Intensity Points

It is well illustrated in Appendix III that the interaction theoretically becomes nil for certain frequency and mode combinations. We have experimentally verified the existence of these "zero points" and obtained excellent agreement with theory. The case that we explored involved the interaction of longitudinal and transverse waves to produce a sum frequency longitudinal beam (Case III). The specimen was a 6 in. diameter disk of magnesium with many flats machined along the circumference to facilitate attainment of resonant conditions for various primary frequency ratios.

Figure 3 illustrates the striking agreement between the experimental and theoretical results after a "normalization" factor is applied to the theoretical curve. As the third-order elastic constants are not known for magnesium, it is not yet possible to calculate the absolute values for quantitative comparison with the experimental results. However, as mentioned earlier, Case III is one of the cases where the general shape of the curve is not influenced by the third-order elastic constants. We can therefore compare the curve shapes without knowledge of the third-order constants.

The experimental data points follow the theoretical curve very closely and confirm the position of the theoretical "zero point." The zero point occurred when the two longitudinal beams (one primary beam and the generated beam) were perpendicular. This condition is, of course, also in agreement with theory.

11
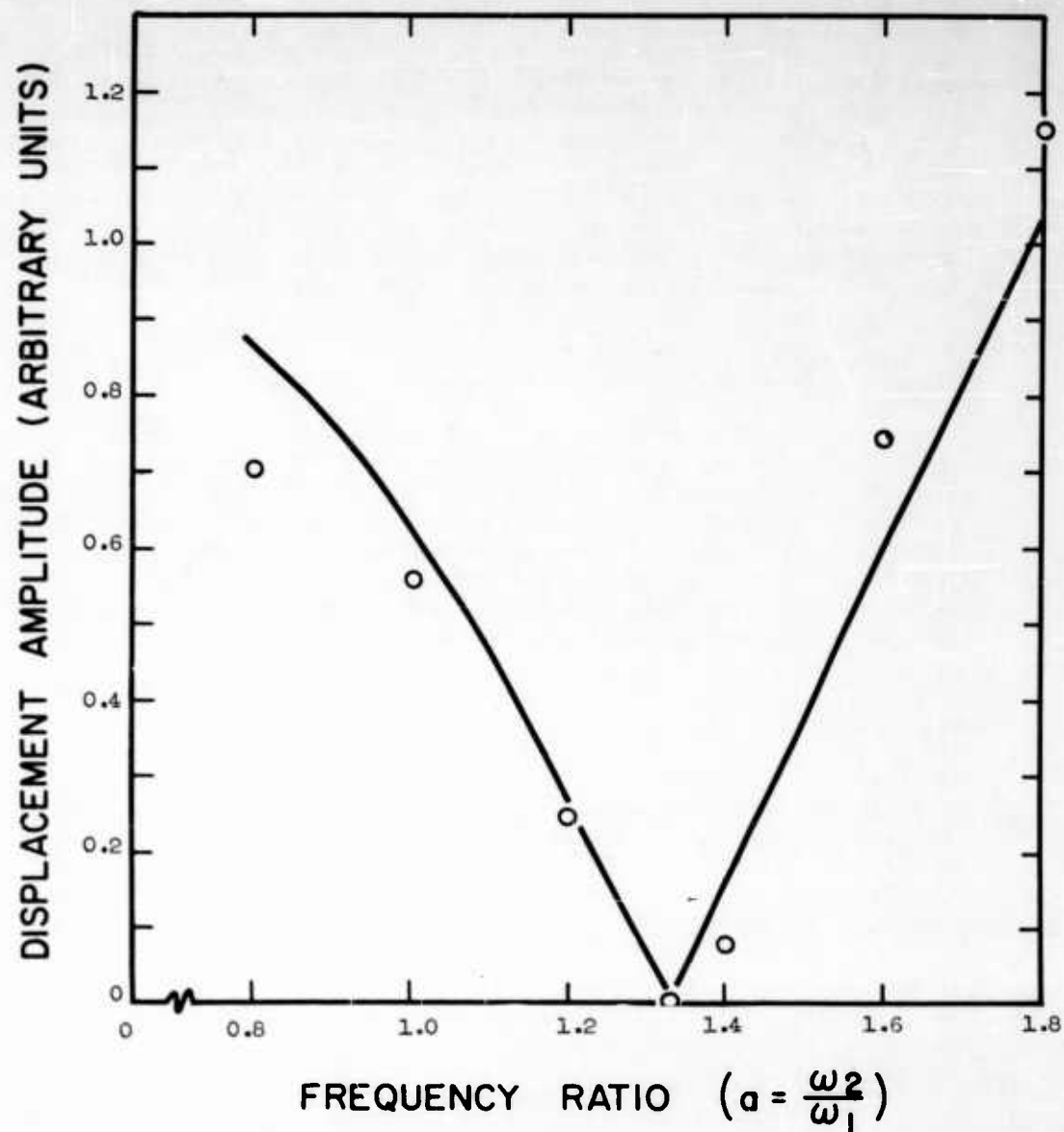
Figure 3 - Displacement Amplitudes for Generated Beams in Case III
Interaction Showing Experimental Data (Open Circles)
and Normalized Theoretical Curve (Solid Line)

12

## E. Dependence on Plastic Deformation

In the theoretical treatment of beam interaction the material is considered to be perfectly elastic although nonlinear effects are of course included. The possibility that dislocations also contribute to interaction effects has been considered and preliminary experiments performed to detect such effects. Figure 4 illustrates one experimental setup. Two 5 Mc shear waves were crossed at the center of a 6 in. diameter disk of 1100 aluminum to produce a 10 Mc longitudinal wave that propagates toward the transducer at position B. Straight across the disk from position B another 10 Mc x-cut transducer was pulsed at 10 Mc simultaneous with the pulsing of the two 5 Mc shear wave transducers. The longitudinal wave packet travels much faster than the two shear waves and it therefore passed through the "interaction zone" prior to arrival of the shear wave packets. Two 10 Mc signals were thus detected by the transducer at position B. The first signal originated at transducer A and the second signal was produced by interaction of the two shear packets. Both signals were displayed on the same oscilloscope trace and initially adjusted for equal amplitude.

Changes in dislocation density, loop length, etc., were produced by applying compressive loads to a small area at the disk center, i.e., at the interaction zone. The deformation area was far enough removed from the disk circumference that surface deformation effects such as loss of parallelism and bond cracking were not noticeable. The first signal (from the opposite 10 Mc transducer) was used primarily as an indication of attenuation effects produced by the dislocation changes in the interaction zone. This signal remained essentially constant whereas the signal from the interaction changed appreciably as the load was applied and removed. The signal from the interaction also varied with time immediately following a variation in load. These results at first appeared to indicate a strong relationship between interaction intensity and dislocation content. However, subsequent observation of the first echo from one of the 5 Mc transducers showed that this signal also varied considerably as the load was changed. This variation may be due to dislocation changes or it might be caused by rotation of the polarization direction in the stress field around the compressed volume. Additional experiments will be necessary to completely pin down the source of the observed changes.
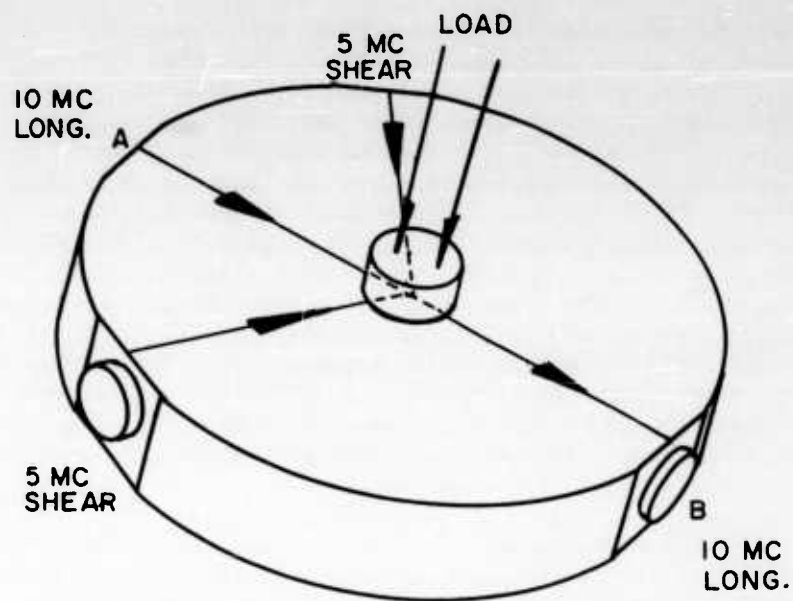
Figure 4 - Experimental Arrangement for Studying the Effect of
Severe Deformation on Magnitude of Interaction

## IV. CRITICALITY OF ANGULAR RELATIONSHIPS DURING INTERACTION

### A. Apparatus

Some preliminary results on the angular spread of the scattered wave were included in a previous report[3]/ but more recent experiments have improved our understanding of all of the angulation and collimation characteristics of the interaction phenomena. The investigation has been greatly facilitated through the use of the apparatus shown in Figure 5. This "ultrasonic goniometer" was designed specifically for interaction experiments in which one or more of the ultrasonic beams can be coupled into (or out of) the specimen through a water bath. A 2-1/2 in. diameter cylindrical shaft is mounted perpendicular to a heavy baseplate and the center of this shaft is an axis of rotation for two immersion type transducers and the diskshaped test specimen. Two transducer holders are attached to heavy rings that fit concentrically about the center shaft. The ring-shaft fit is very close and yet rotation of the rings about the shaft is smooth and easy. The transducer holders are equipped with alignment screws that work against pressure provided by heavy springs. The disk-shaped specimen is waxed onto a cap-like piece that fits snugly over the top of the shaft and also rotates about the shaft axis.

Figure 6 is a schematic presentation that illustrates the versatility of the above equipment. The specimen is shown as a 6 in. diameter disk with a "flat" machined at position A. Shear-mode transducers can be bonded directly to this flat using either solid couplants such as Salol or viscous liquids such as Nonaq. The other two transducers (B and C) are immersiontype units. The central mounting shaft acts as an axis for the independent rotation of the two immersion type transducers as well as the disk-shaped specimen. The apparatus is partially submerged in water to provide suitable coupling between the specimen and the immersion transducers. The arrows in Figure 1 indicate the propagation vectors for a typical experiment, however, each transducer is interchangeable in its role as a transmitter or receiver. The angular positions of the specimen and the two immersion transducers are reproducible to better than one degree.

### B. Angular Spread of Scattered Wave

The first experiments performed on the above apparatus only involved measurements on the "spread" or collimation characteristics of the scattered wave. Two flats were machined on the disk for this experiment so two shear waves could be intersected at the resonant angle to produce a longitudinal wave.
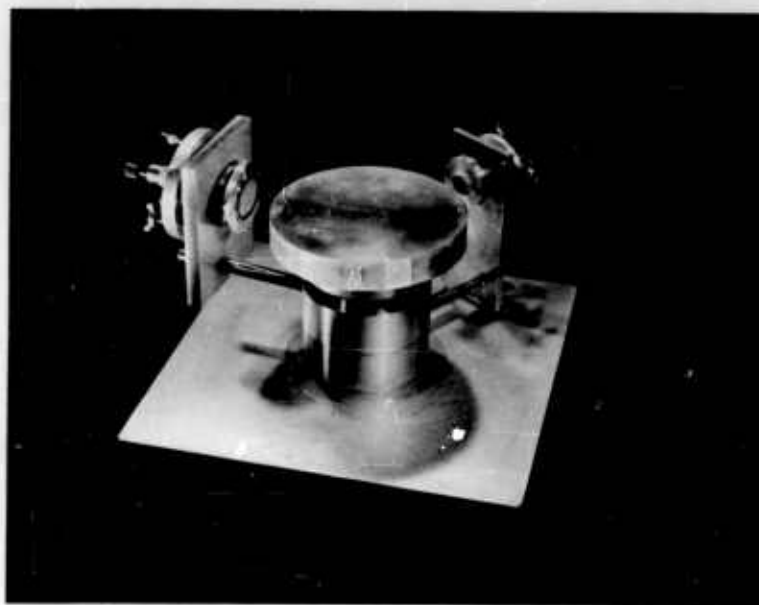
Figure 5 - Apparatus for Performing Interaction Experiments with
Immersion Transducers
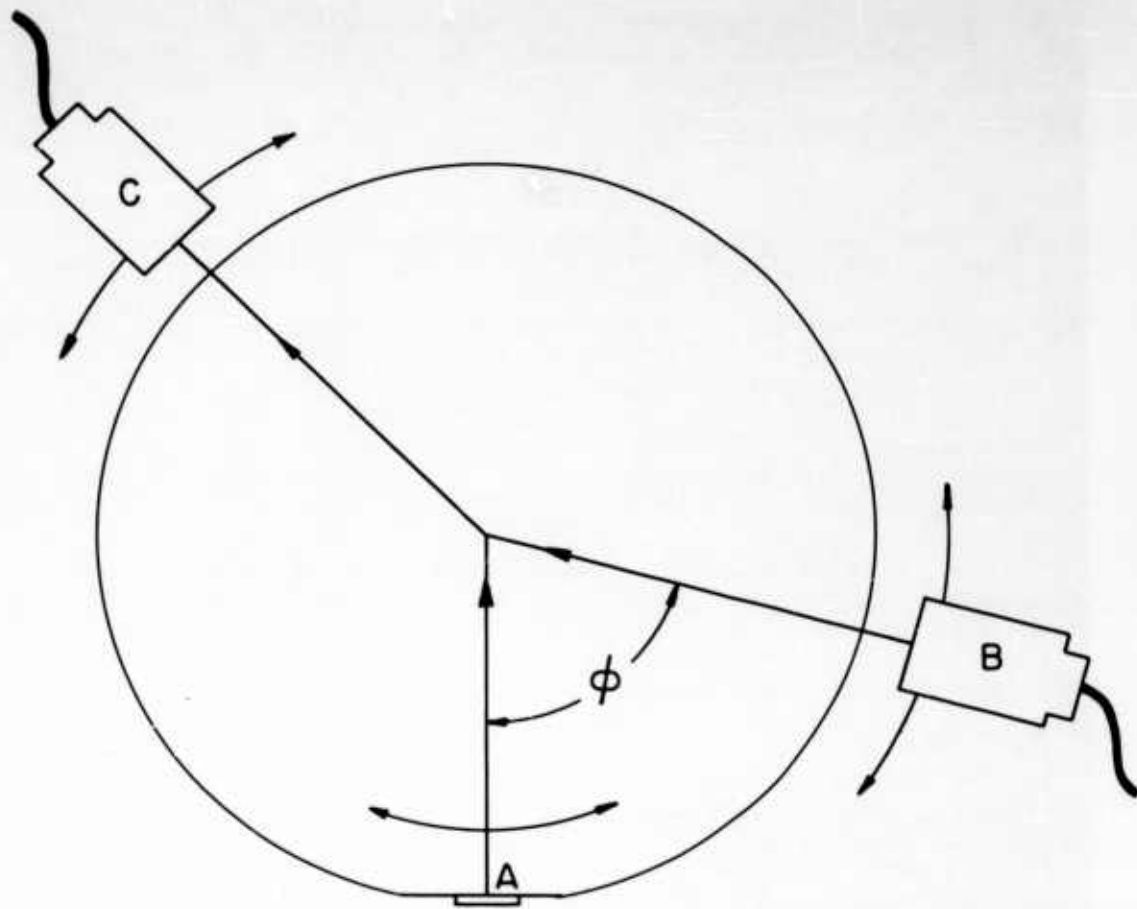
Figure 6 - Schematic Presentation of Variable Angulation Apparatus
for Studying Ultrasonic Beam Interactions

The first case studied was the following interaction:

$$T(5) + T(5) \longrightarrow L(10) \qquad .$$

Interaction occurred at the center of a 6 in. diameter magnesium disk. The scattered wave then traveled through 3 in. of magnesium, was coupled into water at the disk circumference, and was subsequently detected with an immersion transducer. The signal was then observed as the transducer was rotated about an axis which passed through the interaction zone. Maximum signal occurred at the theoretically predicted angle and the angular width of the beam at "half-peak amplitude" was approximately 6°. These results were obtained when the active area of the primary beam transducers was circular with a diameter of 1/2 in.

When the two 5 Mc transducers were driven at their third harmonic (15 Mc), a scattered wave of 30 Mc was detected but the angular width at "half-peak amplitude" was then only about 3°. This apparent increase in beam collimation is probably due to several factors including (1) better collimation and smaller relative bandwidth of the primary beams at the higher frequency, and (2) increase in ratio of interaction zone dimension to wavelength of the scattered wave.

If we consider the interaction region to behave somewhat like a piston source, one might reasonably expect side lobes to be associated with the scattered waves. A search was made for such side lobes by looking for slight increases in the scattered signal amplitude as the transducer was scanned along the "tail" of the gaussian-like response curve. Side lobes were not observed when either the full face of the transducer was used or when an absorbing mask with a 2 mm. wide slit was introduced between the specimen and the transducer. The slit was used in an attempt to increase resolution and thus the sensitivity for detecting slight variations in beam intensity. The actual capability of our equipment to detect side lobes from a piston source was subsequently checked by cutting one of our disk-shaped specimens along a diametral line and mounting a 10 Mc quartz transducer (dia. = 1.1 cm.) at the center of one half. The geometry of our arrangement was thus changed very little except that the transducer, rather than interaction, produced the 10 Mc longitudinal wave that was detected with the immersion transducer. Side lobes were easily detected in this case. The total angular width of the main lobe was measured at approximately 7°. This is in reasonable agreement with the theoretical prediction of about 8°.

It must be admitted that the curved nature of the solid-liquid boundary influences the character of the emerging wave. Nevertheless, the results obtained with the half disk suggest the influence is slight. The apparent lack of side lobes associated with the scattered beam deserves additional study.

C. Angulation of All Three Beams

A series of three interaction cases were investigated for the angular relationship between all three beams. The cases studied were:

$$L(10) + T(5) \longrightarrow L(15)$$

$$L(15) + T(5) \longrightarrow L(10)$$

$$L(15) + L(10) \longrightarrow T(5)$$

All three of the above cases can, of course, be studied with the same three transducers, i.e., two immersion type units having resonant frequencies of 10 Mc and 15 Mc plus one 5 Mc shear-mode crystal blank.

The fact that "scattered" waves were easily detectable in all three of the above mentioned cases is important to the ultimate application of the interaction phenomenon to nondestructive testing. It illustrates that interaction effects can be observed even when two of the three beams involved are coupled into (or out of) the specimen through a liquid medium. To make conditions even more difficult, the liquid-solid boundary was curved. The results thus suggest that interaction may be produced in specimens of rather complex shape using immersion techniques. Even the shear-wave that is always present could possibly be produced (or detected) by using a third longitudinal beam in the liquid medium and planning for the refractive mode conversion that occurs at the boundary.

The preceding section gave some data on the angular spread of the "scattered" beam. Experiments have also been performed to explore the criticality of the resonant angle, $\phi$ , between the two primary beams. Resonant conditions were first established in each case and then the angle between the two primary beams was varied on either side of the optimum angle until the amplitude of the scattered signal dropped to one-half the amplitude under resonant conditions. The total angular change, $\Delta\phi$ , to go from one-half peak amplitude on one side of resonance to one-half peak amplitude on the other side of resonance was found to be $5° \pm 1°$. It can be argued that

19

when $\phi$ is varied from the resonant angle, the position of the scattered wave detector should be altered also since the direction of the scattered wave is defined as $(\overline{k}_1 \pm \overline{k}_2)$ where $\overline{k}_1$ and $\overline{k}_2$ are the propagation vectors of the two primary waves. Attempts were made to observe this effect by rotating the detector slightly after $\phi$ had been varied from the resonance angle. However, we were unable to observe any appreciable recovery in the amplitude of the scattered wave. In interpreting the above results, the frequency bandwidth, as well as the spread and dimensions of the two primary beams must be kept in mind.

The amplitude of the scattered wave was also studied as a function of frequency of one primary beam. The ideal way to perform this experiment would be to attain resonance conditions and then vary the frequency of one primary beam without altering the intensity. Unfortunately, this is very difficult to do with the "resonant" transducers one usually uses in ultrasonic work. Varying the generator frequency away from the natural frequency of the transducer produces rather severe changes in the intensity of the ultrasonic pulse. Some improvement in the "flatness" of the transducer response was achieved by driving it "off-resonance" to start with. Under these conditions the angulation between all transducers was set up for maximum amplitude of the scattered signal. In one such case, we drove the 15 Mc transducer at 12.5 Mc. The amplitude of the scattered wave was then halved by decreasing the primary frequency to 12.0 Mc. However, an increase in frequency to 15.3 Mc was necessary to get similar results. Thus, we see that the crystal resonance still controlled the experimental results.

Even though crystal resonances made it very difficult to vary frequency and maintain intensity, we were able to observe the effect of frequency changes on the required beam angulation for maximum interaction. For example, when a 15 Mc longitudinal beam is interacted with a 5 Mc transverse beam in magnesium, the calculated value of $\phi$ is 40.8°. Our experimental setup verified this condition. If the 15 Mc is changed to 12 Mc, the theoretical value of $\phi$ decreases to 35.7°. After experimentally observing interaction for

$$L(15) + T(5) \longrightarrow L(10) \quad ,$$

the 15 Mc transducer was driven at 12 Mc. The scattered signal had to be amplified more, of course, to remain detectable at this nonresonant condition. The angle $\phi$ was next altered to maximize the scattered signal and then the position of the 10 Mc transducer was varied in the same manner.

After the first try at maximization, very little change in angles was observed even though $\phi$ should theoretically have changed about 5° for the interaction

$$L(12) + T(5) \longrightarrow L(7) \quad .$$

However, we subsequently noticed that, if the 15 Mc transducer and the 10 Mc transducer were alternately positioned for maximum scattered amplitude, the theoretical values were finally obtained after about 10 alterations. Attempts to further maximize the scattered wave amplitude did not produce any additional angular changes.

## V. USE OF INTERACTION TECHNIQUES IN THE STUDY OF ELASTIC ANISOTROPY

A very brief outline of a potential technique for three-dimensional stress analysis using the interaction phenomenon was presented in an earlier report.[3] More recently, we have illustrated the feasibility of this technique under very special circumstances. The large block of magnesium shown in Figure 7 was first examined for elastic anisotropy in the following manne . Two 6 Mc shear crystals were positioned opposite each other to make a transmitter-receiver combination through the 4 in. thickness (z-direction) of the magnesium block. When the transmitter crystal was oriented so that the shear wave was polarized along the x-axis, the receiver signal amplitude was observed as the receiver crystal was rotated. The results indicated that the emergent beam was still plane-polarized along the x-axis. Similarly, when the incident beam was polarized along the y-axis, the emergent beam was also found to be polarized along the y-axis. The lack of apparent rotation suggested that the block was either (1) elastically isotropic or (2) the x- and y-axes were axes of anisotropy. The latter situation was later confirmed by polarizing the incident beam at 45° between the x-axis and y-axis. The emergent beam was then found to be plane-polarized but the plane of polarization had rotated 90° from that of the incident beam. The interaction technique illustrated in Figure 7 was then used to further examine the elastic anisotropy at various points along the thickness (z-axis).

We wished to produce a transverse wave at the intersection point, so the interaction

$$L(\omega_1) + L(\omega_2) \longrightarrow T(\omega_1 - \omega_2)$$

21
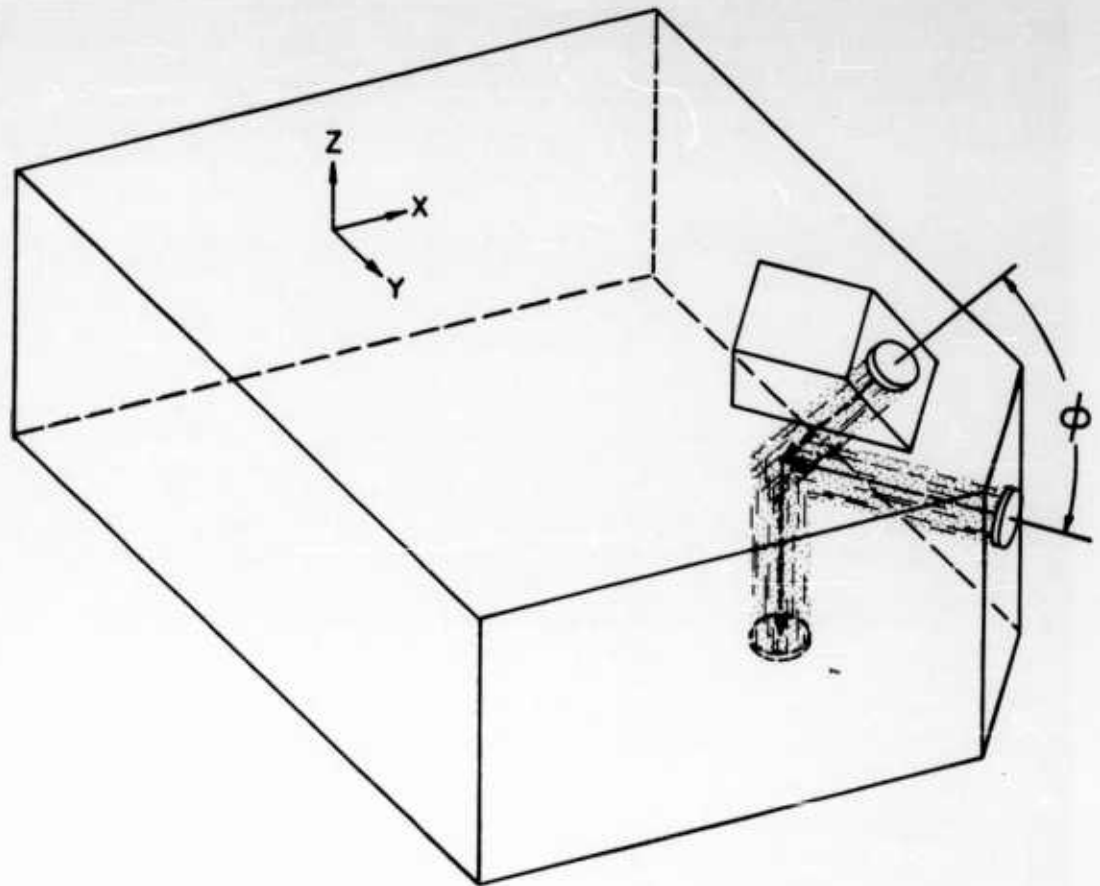
Figure 7 - Magnesium Block with Transducers Mounted
for Interaction Experiment

was chosen. The transverse wave produced by such an interaction is initially
polarized in a plane generated by the propagation vectors of the two primary
beams. In the preceding paragraph we saw that, in order to observe shear-
wave rotation for z-axis propagation, the shear wave should be polarized at
45° to the x- and y-axes. A corner was thus cut off of the block at 45°
(see Figure 7) to permit bonding of one primary transducer. Figure 8 is a
top view and section of the block in which one can easily see the angular re-
lationship between the three beams. The specific interaction,

$$L(14) + L(8) \longrightarrow T(6) \quad ,$$

was selected for this particular experiment because the 8 Mc longitudinal
beam and the 6 Mc shear beam turn out to be perpendicular to each other as
shown in the figure. The 6 Mc beam thus travels perpendicular to the major
faces of the block. The wedge, used to couple the 14 Mc beam into the block,
was also made of magnesium in order to minimize impedance mismatch and re-
fraction at the wedge-block boundary. The 14 Mc x-cut transducer was bonded
to the wedge with Salol but the 8 and 6 Mc crystals and the magnesium wedge
were all coupled to the block with castor oil. This facilitated translation
of both the wedge (14 Mc beam) and the 8 Mc crystal, and rotation of the
6 Mc receiver crystal.

The two primary beams were varied in position such that intersec-
tion always occurred along a single line running through the block thickness
(line ZZ in Figure 8). When the intersection point was within 1/4 in. of the
top surface we obtained results almost identical to those observed when two
6 Mc crystals were used as a transmitter-receiver pair, i.e., a 90° rotation
of the plane of polarization occurred as the shear wave traveled through the
thickness of the block. As the intersection point was moved down along ZZ
in 1/2 in. intervals, the shear wave arriving at the receiving crystal gen-
erally had an elliptical character to the particle motion. The ellipticity
was roughly determined by using the AC-cut quartz crystal as an analyzer,
and comparing the signal amplitude produced when the sensitive axis of the
crystal was alternately rotated along the major and minor axes of the
ellipse. For propagation through the entire thickness we essentially ob-
served a line ellipse with a 90° rotation of the plane of polarization.
Table 3 contains the relative magnitudes of the maximum and minimum signal
observed as the receiver crystal was rotated. The elastic anisotropy is
seen to be relatively uniform through the thickness of the block. Note that
when intersection occurred midway through the block, the emergent shear wave
was almost circularly polarized. The results also show that in our original
experiment, where two 6 Mc crystals were used for propagation through the
entire thickness, the 90° rotation of the plane of polarization corresponds
to a phase retardation between the component waves of 180° rather than some
odd-integer multiple of 180°.

23

(a) TOP VIEW

WEDGE

(b) SECTION A-A
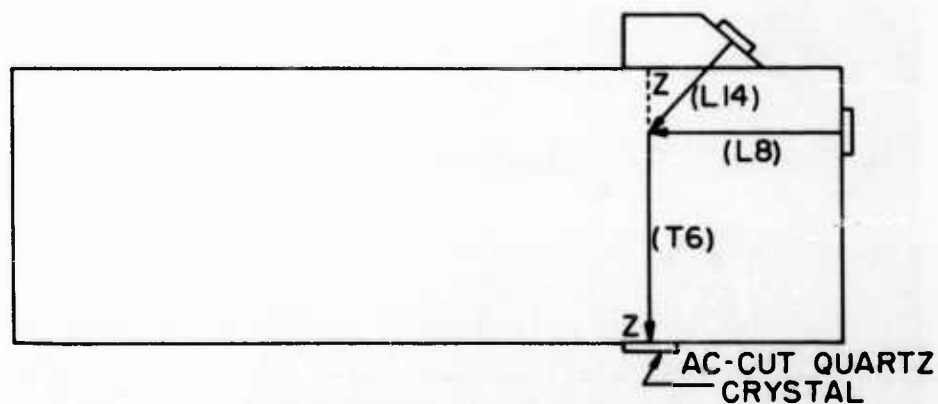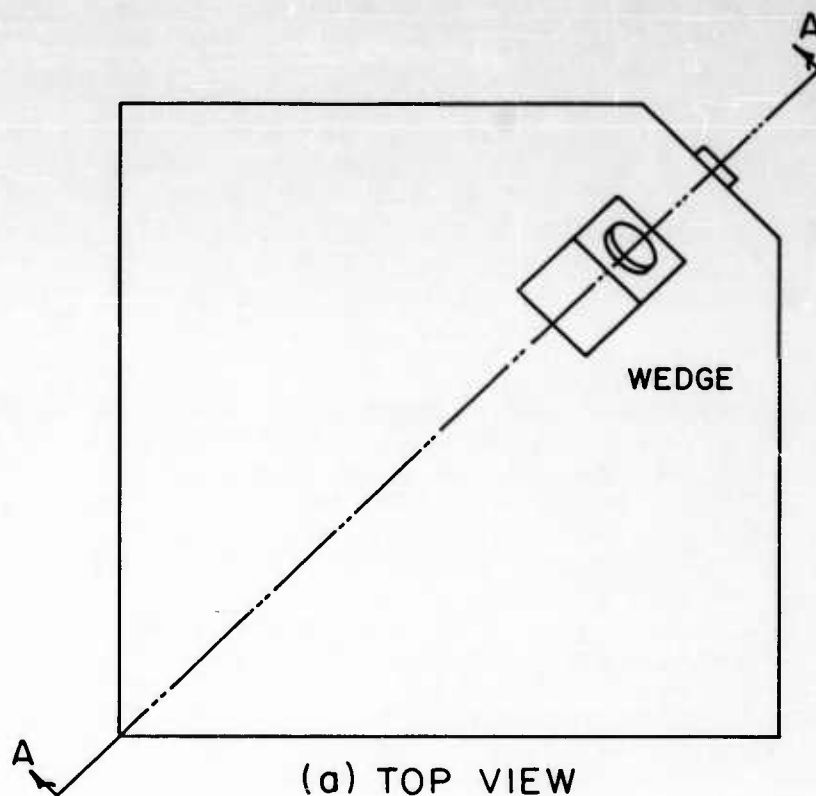
Figure 8 - Top View of Block and Section Through Plane of Interaction
Showing Single Wedge Technique

24

## TABLE 3

| Distance of Intersection Point From Top of Block in Inches | Relative Amplitude When Sensitive Axis of Receiver was Parallel to Plane of Interaction | Relative Amplitude When Sensitive Axis of Receiver was Perpendicular to Plane of Interaction |
|:---:|:---:|:---:|
| 0.5 | ~1 | 10 |
| 1.0 | 3 | 10 |
| 1.5 | 6 | 10 |
| 2.0 | 9 | 10 |
| 2.5 | 10 | 5 |
| 3.0 | 10 | 3 |
| 3.5 | 10 | < 1 |

Although there is much room for improvement in the foregoing experiment, it illustrates the feasibility of using interaction techniques to study elastic anisotropy on a three-dimensional basis. Residual stresses can, of course, produce or contribute to such anisotropies.

The interaction case used in the previous experiment is somewhat limited because the plane of interaction is not readily variable. A much more versatile arrangement is illustrated in Figure 9. The use of two wedges will facilitate continuous rotation of the plane of interaction (and thus the initial polarization of the generated shear wave). The principal axes of anisotropy can thus be determined and a suitable calibration would permit determination of the degree of anisotropy.
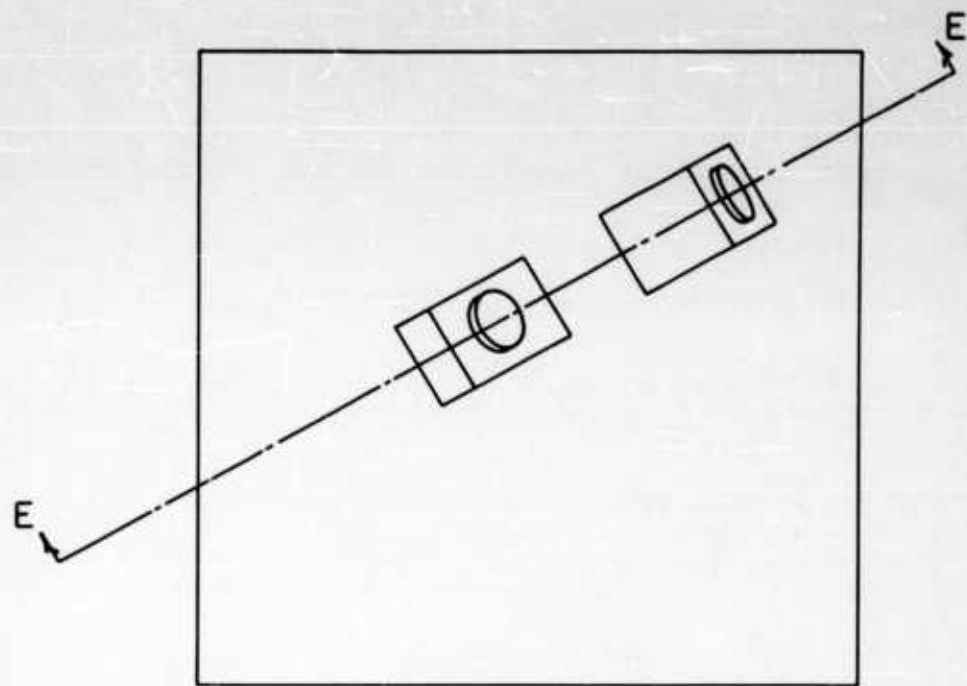
(a) TOP VIEW
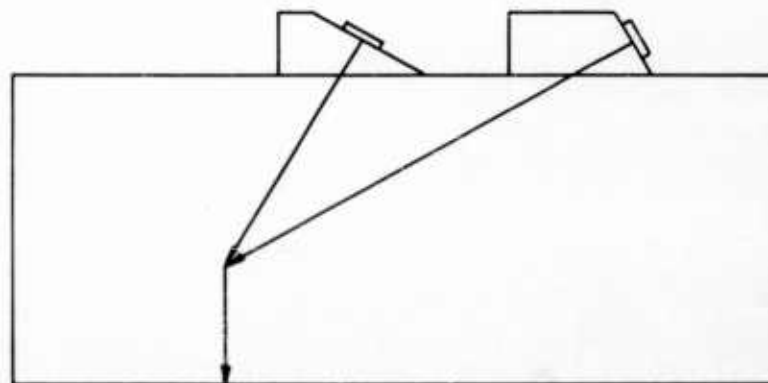


(b) SECTION E-E

Figure 9 - Top View of Block With Section Through Plane of Interaction
Showing Double Wedge Technique

26

## REFERENCES

1. Rollins, F. R., WADD Technical Report, 61-42, Part I (1961).

2. Rollins, F. R., Kobett, D., and Jones, G. L., WADD Technical Report, 61-42, Part II (1962).

3. Rollins, F. R., and Waldow, P., WADD Technical Report, 61-42, Part III (1963).

4. Smith, R. T., Ultrasonics, 1, 135 (1963).

5. Jones, G. L, and Kobett, D., J. Acoust. Soc. Am., 35, 5 (1963).

6. Rollins, F. R., Applied Physics Letters, 2, 147 (1963).

7. Fleury, P. A., and Alers, G. A., Ford Motor Company, Scientific Laboratory Report, SL 1-116.

8. Ziman, J. M., Electrons and Phonons, Oxford Press, p. 129 (1962).

9. Seeger, A., and Buck, O., Zeitschrift für Naturforschung, 15, 1056 (1960).

APPENDIX I

GLOSSARY OF TERMS

All variables with a numerical subscript have the meaning given by
the variable symbol but pertain only to the waves designated by the subscript
number. The glossary is not complete but contains terms which may be re-
ferred to frequently.

A,B,C - third-order elastic constants

$a$ - ratio of primary frequencies $\dfrac{\omega_2}{\omega_1}$

$c_t$ - velocity of shear wave

$c_\ell$ - velocity of longitudinal wave

$c$ - ratio of velocities $\dfrac{c_t}{c_\ell}$

$\hbar$ - Planck's constant divided by $2\pi$

$K$ - bulk modulus

$\bar{k}$ - propagation vector

$\ell^2$ - cross-sectional area of square beam

$L(\omega)$ - longitudinal wave of frequency $\omega$

$m$ - mass of a volume of interaction

$N$ - number of interacting phonons

$r$ - distance between point of intersection and point of
observation

$R^3$ - "volume" occupied by one phonon

$T(\omega)$ - transverse wave of frequency $\omega$

$V$ - volume of intersection

$X$ - displacement amplitude

$\omega$ - angular frequency

$\rho$ - density

$\mu$ - shear modulus

$\phi$ - angle between primary waves at resonance

$\alpha$ - angle between first wave and scattered wave

$\theta$ - angle between polarization direction and plane of inter-
action

$\delta$ - intermediate variable defined in Appendix III

30

APPENDIX II

RELATIONSHIP BETWEEN TRANSITION PROBABILITY AND WAVE AMPLITUDE

In this appendix an approximate relationship between the transition probability and the classical amplitude of the scattered wave is obtained. The derivation is admittedly rough but a more refined calculation does not seem to be warranted until more accurate information is available on the third-order elastic constants and the measurable nonlinear effects.

Let us envision a classical elastic wave packet of square cross section, $\ell^2$ , as being an ideally dense homogeneous beam of phonons. The intensity of the beam is given as

$$I_1 = \rho_1 \hbar \omega_1 c_1$$

where $\hbar$ is Planck's constant divided by $2\pi$ , $\rho_1$ is the phonon density and $c_1$ is the speed of beam 1. The well known classical expression for the intensity is given by

$$I_1 = \frac{1}{2} \left( \rho c_1 \omega_1^2 X_1^2 \right)$$

where $\rho$ is the density of the material and $X_1$ is the classical displacement amplitude. Thus

$$\rho_1 = \frac{\rho \omega_1}{2\hbar} X_1^2 \quad .$$

Each phonon can be considered as occupying a cube of space, $R_1^3 = \frac{1}{\rho_1}$ . Now consider one such space cube located in the volume of interaction but having a fixed position. In $dt$ seconds, $\rho_2 c_2 R_1^2 dt$ phonons of the second beam and $\rho_1 c_1 R_1^2 dt$ phonons of the first beam transverse this space cube. Consequently, as $dt \rightarrow 0$ , $\frac{\rho_2 c_2}{\rho_1 c_1}$ phonons of the second beam interact with each phonon of the first beam. In other words, the phonon numbers for the initial state are given by

$$N_1 = 1 \ , \ N_2 = \frac{\rho_2 c_2}{\rho_1 c_1} \ , \ N_3 = 0 \quad .$$

Assuming large beam lengths, so that end effects can be disregarded, the total number of phonons in the scattered beam, $n_3$ , is given by

$$n_3 = \rho_1 V W_1 T \quad ,$$

where $V$ is the volume of interaction, $T$ is the total time of interaction between the two beams, and $W_1$ is the transition probability per unit time for one phonon of the first beam undergoing a transition to a higher or lower energy state. However, $n_3$ is also given by

$$n_3 = \rho_3 L_3 A_3 \quad ,$$

where $L_3$ is the length of the scattered beam and $A_3$ is its cross-sectional area. Of course,

$$L_3 = c_3 T \quad .$$

Combining the last three equations, we obtain

$$\rho_3 = \left( \frac{V}{A_3} \right) \frac{\rho_1 W_1}{c_3} \quad .$$

Expressed in terms of amplitudes this equation becomes

$$\chi_3^2 = \left( \frac{V}{A_3} \right) \frac{\omega_1 W_1}{\omega_3 c_3} \chi_1^2 \quad .$$

Assuming $V$ is the geometrical volume of interaction the value of $V$ and $\frac{V}{A_3}$ can be determined from the interaction geometry as diagrammed in Figure 10.
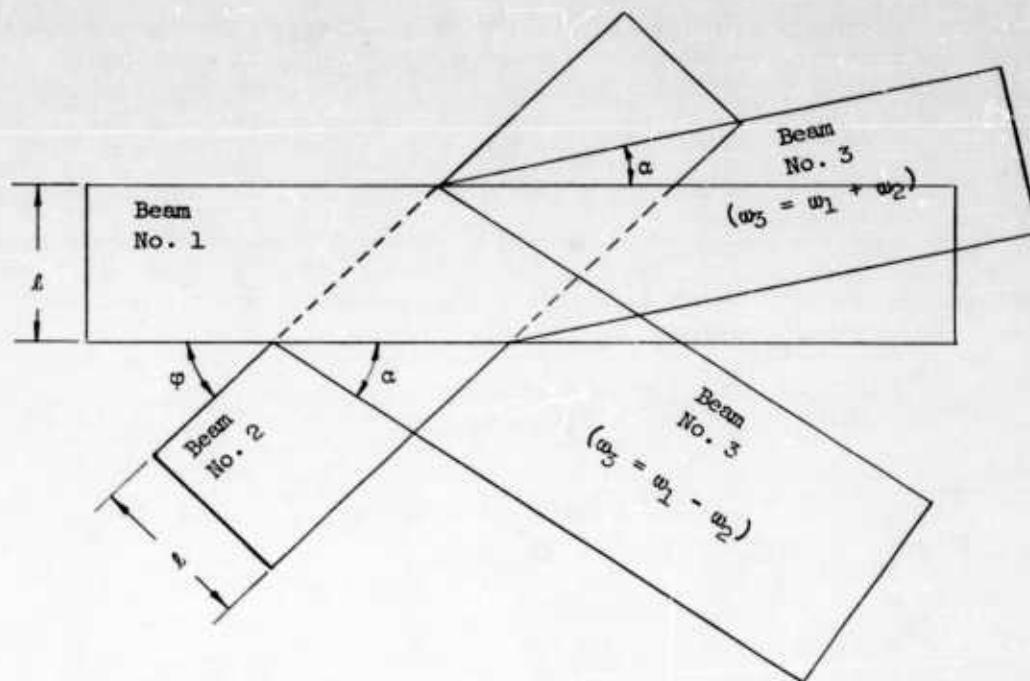
Figure 10 - Geometry of Interaction - In Sum Frequency Cases the
Upper Beam No. 3 is Emitted While in Difference
Frequency Cases the Lower Beam No. 3 is Emitted.

Omitting the geometrical details, we obtain

$$V = \ell^3 \csc \varphi \,,$$

$$\frac{V}{A_3} = \frac{\ell}{\cos \alpha \sin \varphi + \sin \alpha \, (1 - \cos \varphi)} \quad \text{when } \omega_3 = \omega_1 + \omega_2$$

or $$\frac{V}{A_3} = \frac{\ell}{\cos \alpha \sin \varphi + \sin \alpha \, (1 + \cos \varphi)} \quad \text{when } \omega_3 = \omega_1 - \omega_2 \quad .$$

34

The calculation of $V$ is included since the classical amplitude expressions contain this factor.[5] These very rough calculations are not valid for $\varphi = 0°, 180°$ .

The transition probability per unit time is all that remains to be evaluated. The conventional equation for this evaluation is[8]

$$W_1 = \frac{2\pi}{\hbar} \frac{\sin \frac{Et}{\hbar}}{\pi E} \left| < i \mid H_{pert} \mid f > \right|^2$$

where $t$ is the time duration of the interaction. The $H_{pert}$ is the pertubing Hamiltonian and $< i \mid H_{pert} \mid f >$ is the matrix element between the initial and final states. The matrix elements for all interaction cases can be determined in a straightforward, if laborious, manner.* For large $t\omega_3$

$$\frac{\sin \frac{Et}{\hbar}}{\pi E} \longrightarrow \frac{1}{\hbar \omega_3} \delta(\omega_3 = \omega_1 \pm \omega_2) \quad .$$

Consequently we have

$$\chi_3^2 = \left(\frac{V}{A_3}\right) \frac{2\pi \omega_1}{\hbar^2 \omega_3^2 c_3} \quad \chi_1^2 \left| < 1 , \frac{\rho_2 c_2}{\rho_1 c_1} , 0 \mid H_{pert} \mid f > \right|^2 \quad .$$

This is the equation used to determine the quantum mechanical results of this report.

_____

* Caution should be exercised in this evaluation. Many of the perturbing Hamiltonians published in the literature are incorrect.

APPENDIX III

SCATTERED WAVE AMPLITUDES PREDICTED BY THE CLASSICAL
AND QUANTUM MECHANICAL THEORIES

All of the scattered wave amplitudes* predicted by the classical and quantum theories are listed in this appendix. The expressions include the approximate value of the interaction volume as calculated in Appendix II. In addition to the amplitude expressions the equations for $\cos \varphi$ and $\tan \alpha$ are listed under each case. As previously stated, $\varphi$ is the angle between the propagation direction of the No. 1 wave and the propagation direction of the No. 2 wave. The angle $\alpha$ is the angle between the propagation direction of the No. 1 wave and that of the scattered, or No. 3, wave. Both angles are defined such that they lie between 0° and 180°.

All of the amplitude expressions were programmed for the IBM 1620 computer and calculations were made for polystyrene, pyrex, copper, iron, and REX 535 nickel-steel. These five materials are the only ones for which the third-order elastic constants are known.[4,9] On the basis of physical properties, these five materials could be grouped into two classes: (1) polystyrene and pyrex; and (2) copper, iron, and nickel-steel. An interesting result of the computer calculations is that, on the basis of nonlinear effects, the following two classes seem to be warranted: (1) polystyrene and iron; and (2) pyrex, copper, and nickel-steel.

As examples of the predicted effects, graphs of the computer results for pyrex and iron are given in each case directly opposite the mathematical expressions. The values predicted by the quantum theory are always about two orders of magnitude lower than those predicted by the classical theory. The values for $a = 1$ ($\varphi = 0$) in Case II are omitted since the approximate values of the interaction volume are not valid at this point. The value of $a$ is also limited to those which give a real value for $\varphi$. In reading the graphs it is important to remember that absorption has been neglected.

These graphs were obtained by assuming the following typical experimental conditions. Both input transducers are driven with a voltage of 4,000 v. The frequency of the $\omega_1$ transducer is set at 10 mc. and the frequency of the other transducer is varied to give the stated value of $a$. The following numerical data, in c.g.s. units, were also used:

---

* Absolute values only.

$$\ell = 0.908 \qquad r = 1$$

Pyrex:  $\rho = 2.32$ $\qquad \mu = 2.75 \times 10^{11}$

$\lambda = 1.353 \times 10^{11}$ $\qquad K = 3.186 \times 10^{11}$

$A = 42 \times 10^{11}$ $\qquad B = -11.8 \times 10^{11}$

Iron:  $\rho = 7.87$ $\qquad \mu = 8.2 \times 10^{11}$

$\lambda = 11 \times 10^{11}$ $\qquad K = 16.47 \times 10^{11}$

$A = 110 \times 10^{11}$ $\qquad B = -158 \times 10^{11}$

The value of  r  does not satisfy the validity conditions[5] for the classical equations but it does permit a more valid comparison between the two theoretical calculations.

## Case IA

Two transverse waves interacting to produce a scattered longitudinal wave of sum frequency.



$$\theta_1 = \theta_2 = \frac{\Pi}{2}$$
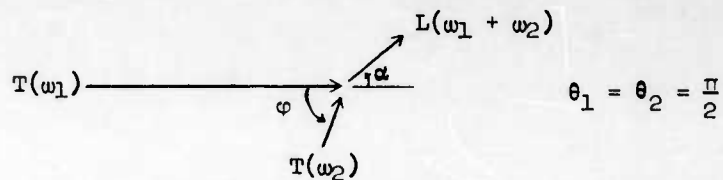
$$\cos \varphi = c^2 + \left[(c^2 - 1)(a^2 + 1)/2a\right]$$

$$\tan \alpha = \frac{a \sin \varphi}{1 + a \cos \varphi}$$

$$\delta_1 = \left\{(B + K - \frac{2\mu}{3})c^2(1 + a)^2 \cos \varphi + (2\mu + A/2)\left[a + (1 + a^2) \cos \varphi + a \cos^2 \varphi\right]\right\}$$

### Classical Result

$$X_3 = X_1 X_2 \delta_1 \omega_1^3 \ell^3 a \csc \varphi \Big/ 8\pi r \rho c_t^4 c_\ell (1+a)$$

### Quantum Mechanical Result

$$X_3 = X_1 X_2 \delta_1 \omega_1^{3/2} \left[a \Big/ \rho c_t^4 (1+a)^2\right] \sqrt{\pi c_\ell \ell \csc \varphi \Big/ 8(1+a)}$$

40

CASE IA

—— Classical Theory

– – – Quantum Theory (x $10^2$)

Pyrex

Iron

Displacement Amplitude $|X_3|$

Angstrom Units

Frequency Ratio ($\omega_2/\omega_1$)

Pyrex Input: $X_1 = 51.6$ Å          Iron Input: $X_1 = 15.5$ Å
$X_2 = 51.6$ Å                        $X_2 = 15.5$ Å

41
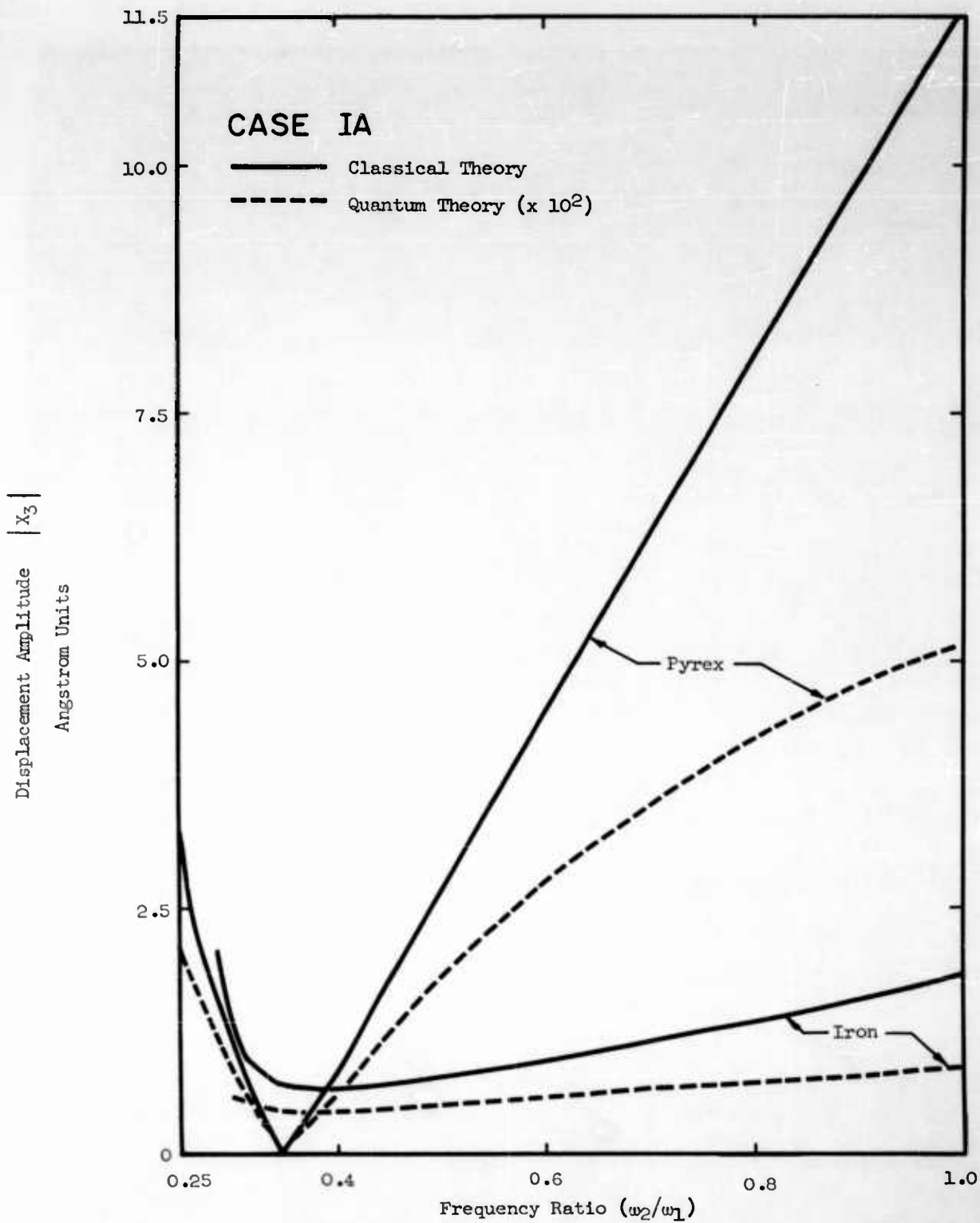
## Case IB

Two transverse waves interacting to produce a scattered longitudinal wave of sum frequency.
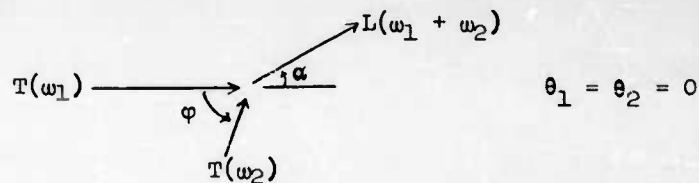


$$\cos \varphi = c^2 + \left[ (c^2 - 1)(a^2 + 1)/2a \right]$$

$$\tan \alpha = \frac{a \sin \varphi}{1 + a \cos \varphi}$$

$$\delta_2 = \left[ (2B + K + A + \frac{7\mu}{3}) \cos^2 \varphi - (B + \mu + \frac{A}{2}) \right]$$

### Classical Result

$$X_3 = X_1 X_2 \delta_2 \omega_1^3 a \, (1+a) \, \ell^3 \csc \varphi \left/ 8\pi r \rho c_t^2 c_\ell^3 \right.$$

### Quantum Mechanical Result

$$X_3 = X_1 X_2 \delta_2 \omega_1^{3/2} (a/\rho c_t^2 c_\ell^2) \sqrt{\pi c_\ell \ell \csc \varphi / 8(1+a)}$$

CASE IB

Classical Theory
Quantum Theory (x 10²)

Pyrex

Iron

Displacement Amplitude $|X_3|$
Angstrom Units

Frequency Ratio ($\omega_2/\omega_1$)

Pyrex Input: $X_1 = 51.6$ Å          Iron Input: $X_1 = 15.5$ Å
$X_2 = 51.6$ Å                                      $X_2 = 15.5$ Å

43
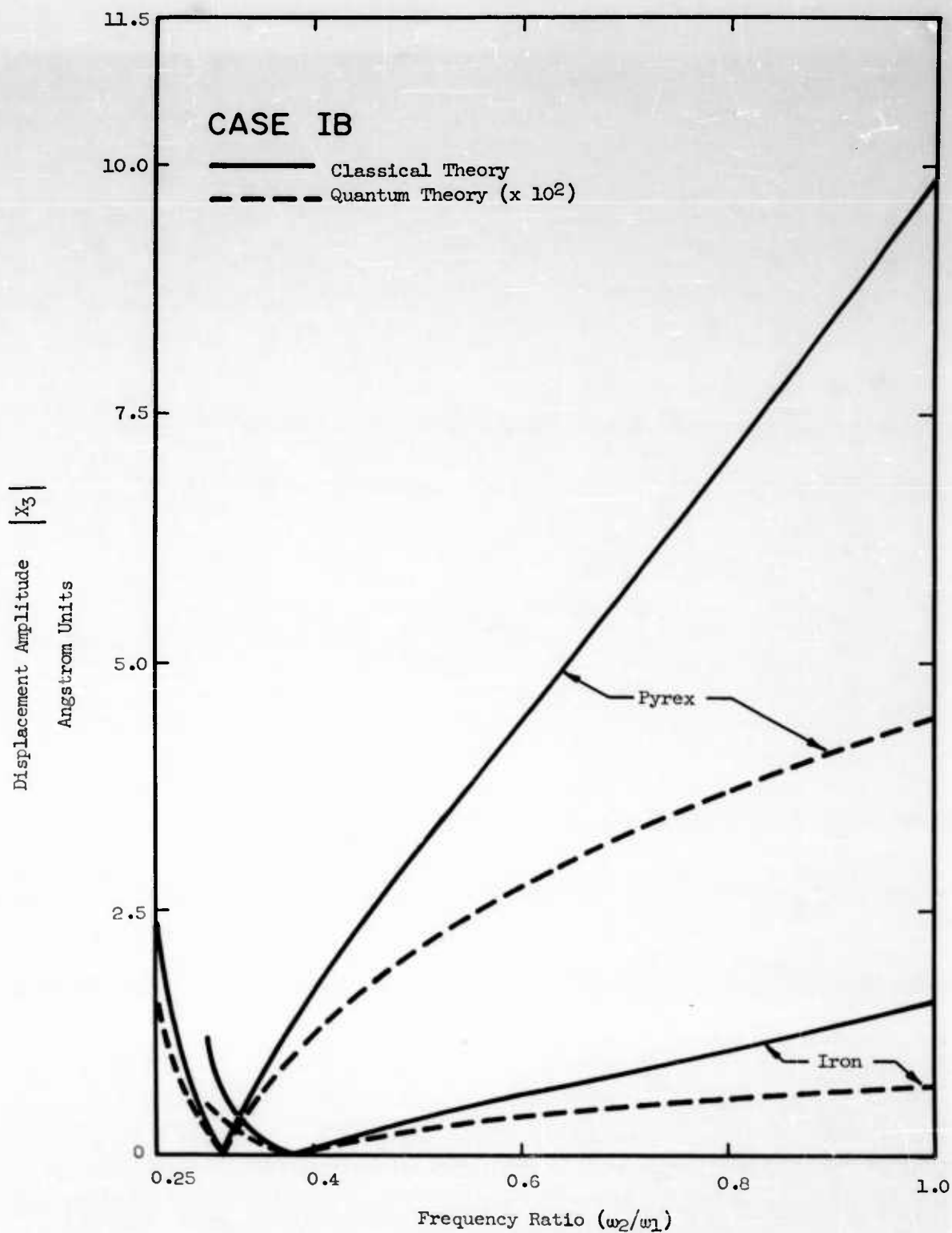
## Case II

Two longitudinal waves interacting to produce a scattered transverse wave of difference frequency.

$$L(\omega_1) \longrightarrow \qquad \theta_3 = 0$$

$$\varphi \qquad \alpha$$

$$L(\omega_2) \qquad T(\omega_1 - \omega_2)$$
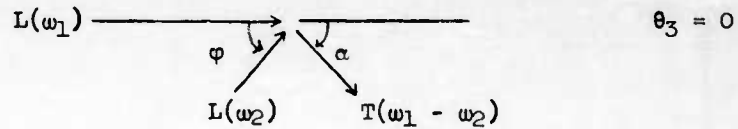
$$\cos \varphi = 1/c^2 + \left[ (c^2 - 1)(a^2 + 1)/2ac^2 \right]$$

$$\tan \alpha = \frac{a \sin \varphi}{1 - a \cos \varphi}$$

$$\delta_3 = (2B + A + K + \frac{7\mu}{3}) \cos \varphi$$

Classical Result

$$X_3 = X_1 X_2 \delta_3 \omega_1^3 a(1+a)\ell^3 \Big/ 8\pi r \rho c_t c_\ell^4$$

Quantum Mechanical Result

$$X_3 = \left[ X_1 X_2 \delta_3 \omega_1^{3/2} \Big/ 8\rho(1-a)c_\ell^4 \right] \sqrt{8\pi(a+X_1^2/X_2^2)a(1+a)c_t \ell} \sin \varphi$$

44

CASE II

Classical Theory
Quantum Theory (x $10^2$)

Displacement Amplitude $|X_3|$

Angstrom Units

Pyrex

Iron

Frequency Ratio ($\omega_2/\omega_1$)

Pyrex Input:  $X_1 = 20.5$ Å        Iron Input:  $X_1 = 5.77$ Å
$X_2 = 20.5$ Å                    $X_2 = 5.77$ Å

45
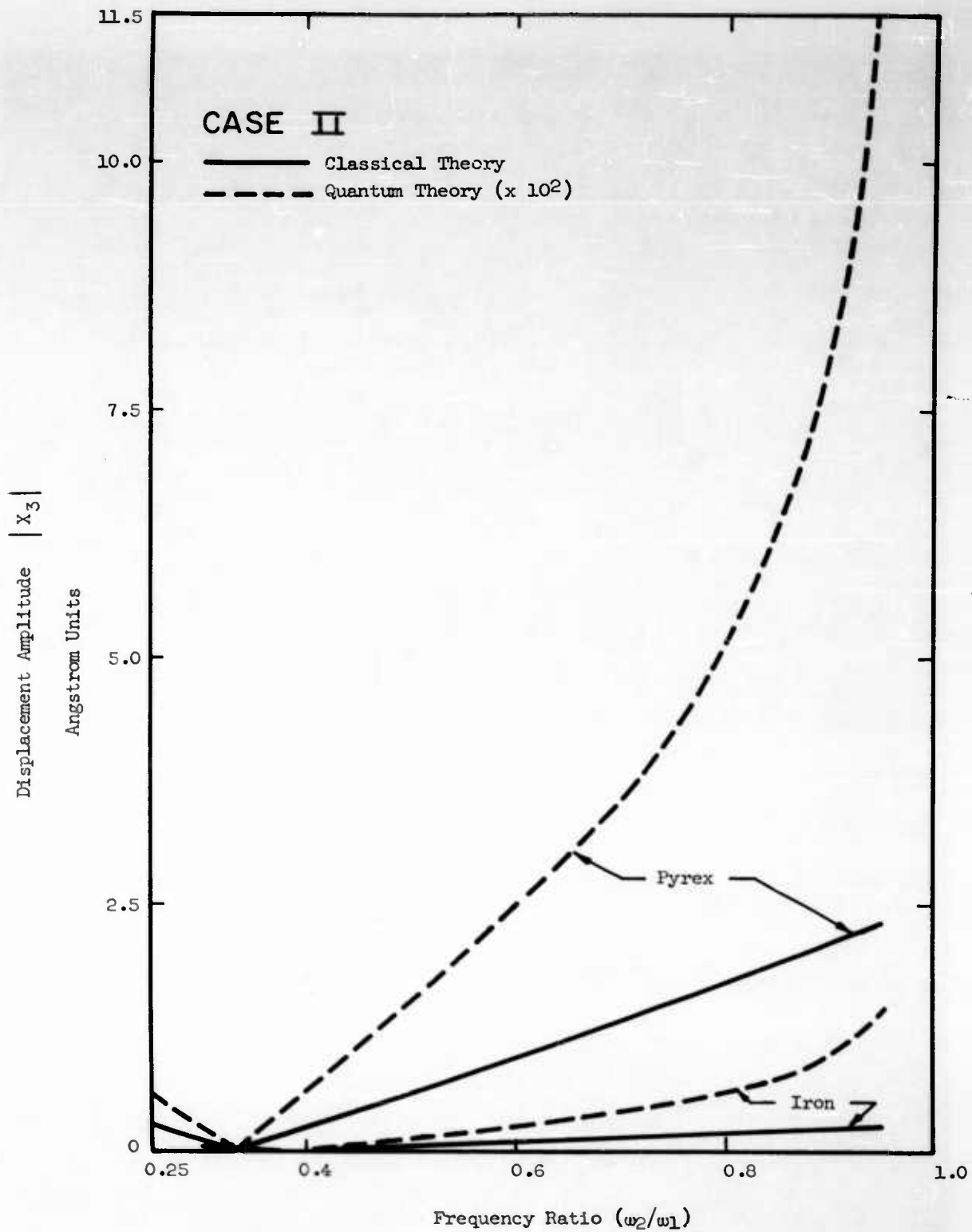
## Case III

A longitudinal wave interacting with a transverse wave to produce a scattered longitudinal wave of sum frequency.
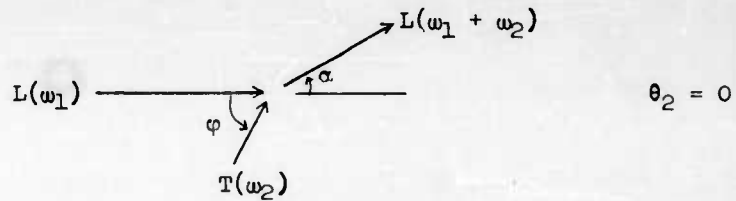


$$\cos \varphi = c + \left[a(c^2 - 1)/2c\right]$$

$$\tan \alpha = \frac{a \sin \varphi}{c + a \cos \varphi}$$

$$\delta_4 = (2B + A + K + \frac{7\mu}{3}) \left[a + c \,(2 + 2a + a^2) \cos \varphi\right]$$

Classical Result

$$X_3 = X_1 X_2 \delta_4 \omega_1^3 a \, \ell^3 \Big/ 8\pi r \rho c_t^2 c_\ell^3 (1+a)$$

Quantum Mechanical Result

$$X_3 = X_1 X_2 \delta_4 \omega_1^{3/2} \left[a \Big/ \rho c_t c_\ell^3 (1+a)^2\right] \sqrt{\pi c_\ell \ell \, \sin \varphi / 8(a+c)}$$

46

CASE III

— Classical Theory
- - - Quantum Theory (x $10^2$)

Displacement Amplitude $|X_3|$ Angstrom Units

Frequency Ratio ($\omega_2/\omega_1$)

Pyrex Input: $X_1 = 20.5$ Å
$X_2 = 51.6$ Å

Iron Input: $X_1 = 5.77$ Å
$X_2 = 15.5$ Å

47
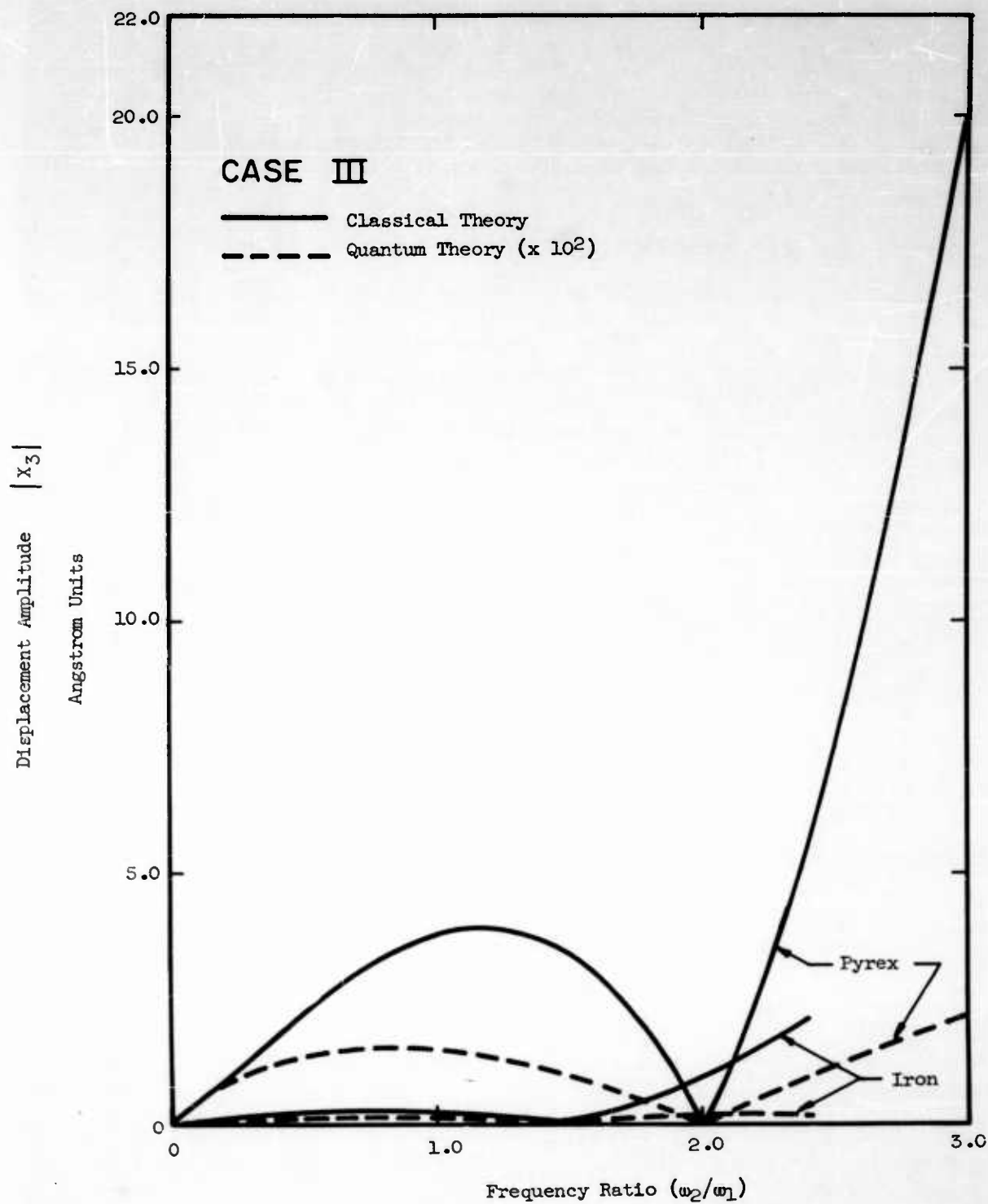
## Case IV

A longitudinal wave interacting with a transverse wave to produce a scattered longitudinal wave of difference frequency.

$$L(\omega_1) \longrightarrow \qquad\qquad \theta_2 = 0$$

$$\varphi \qquad \alpha$$

$$T(\omega_2) \qquad L(\omega_1-\omega_2)$$
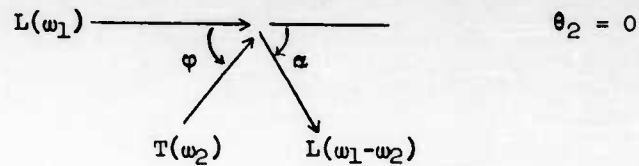
$$\cos \varphi = c + \left[ a(1 - c^2)/2c \right]$$

$$\tan \alpha = \frac{a \sin \varphi}{c - a \cos \varphi}$$

$$\delta_5 = (2B + A + K + \frac{7\mu}{3}) \left[ -a + c \ (2 - 2a + a^2) \cos \varphi \right]$$

### Classical Result

$$X_3 = X_1 X_2 \delta_5 \omega_1^3 a \ \ell^3 \Big/ 8\pi\rho c_t^2 c_\ell^3 (1-a)$$

### Quantum Mechanical Result

$$X_3 = \left[ X_1 X_2 \delta_5 \omega_1^{3/2} \Big/ \rho c_t^2 c_\ell^2 (1-a)^2 \right] \sqrt{\pi(ac + \frac{x_1^2}{x_2^2})ac_t \ell \ \sin \varphi \Big/ 8(a+c)}$$

48

CASE IV

——————— Classical Theory

— — — — Quantum Theory (x 10²)

Displacement Amplitude |X₃|
Angstrom Units

Pyrex

Iron

Frequency Ratio (ω₂/ω₁)

Pyrex Input:  $X_1 = 20.5$ Å      Iron Input:  $X_1 = 5.77$ Å
              $X_2 = 51.6$ Å                    $X_2 = 15.5$ Å

49
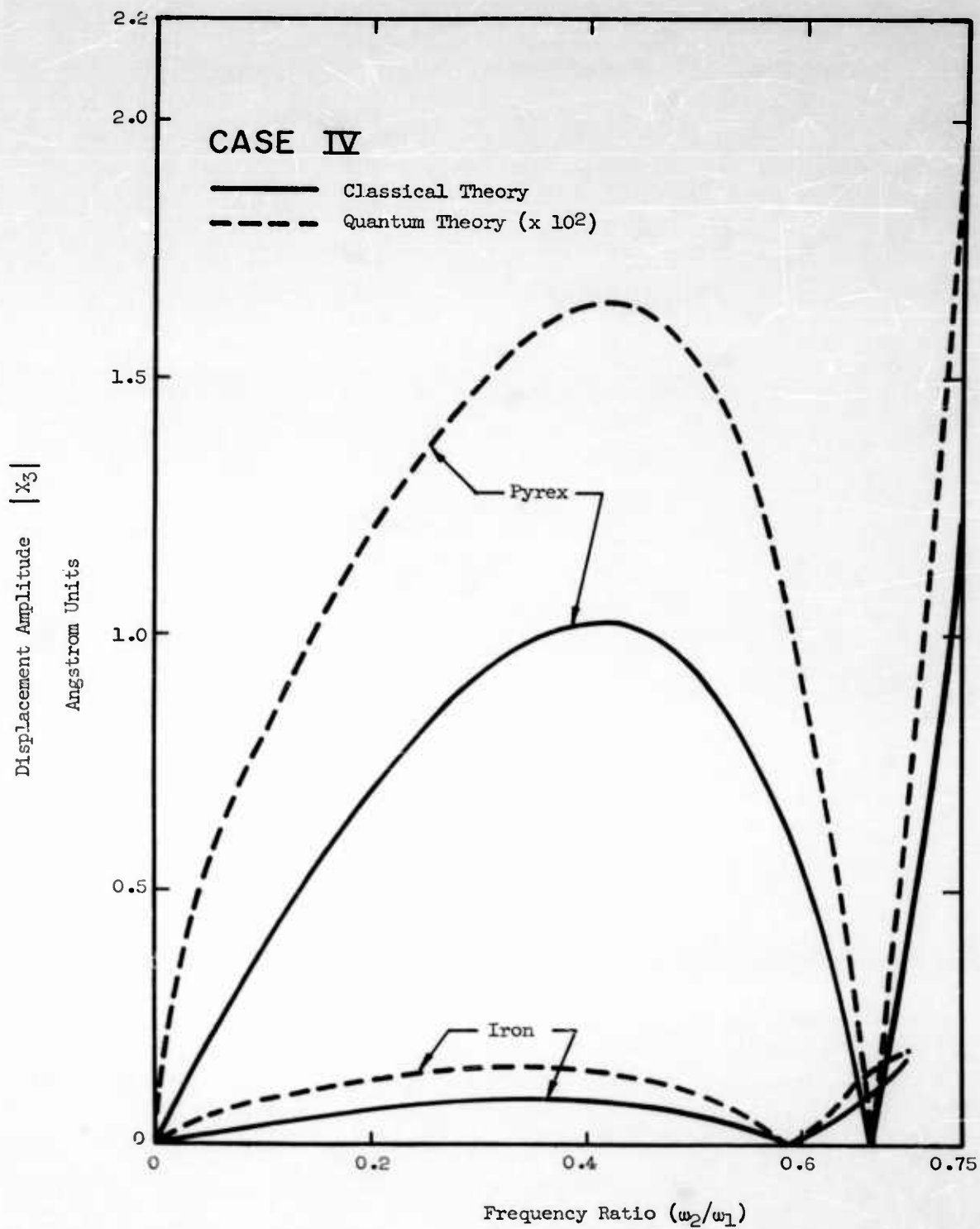
## Case VA

A longitudinal wave interacting with a transverse wave to produce a scattered transverse wave of difference frequency.

$$L(\omega_1) \longrightarrow \qquad \varphi \qquad \alpha \qquad\qquad \theta_2 = \theta_3 = \frac{\pi}{2}$$

$$T(\omega_2) \qquad\qquad T(\omega_1 - \omega_2)$$
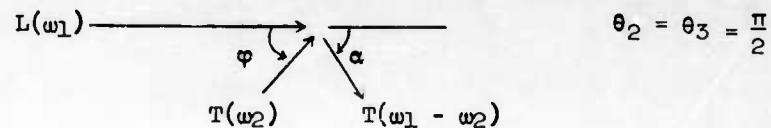
$$\cos\varphi = 1/c + \left[(c^2 - 1)/2ac\right]$$

$$\tan\alpha = \frac{a\,\sin\varphi}{c - a\,\cos\varphi}$$

$$\delta_6 = \left[(B + K - \frac{2\mu}{3})(c\,\cos\varphi - a) + (2\mu + \frac{A}{2})(c - a\,\cos\varphi)\,\cos\varphi\right]$$

Classical Result

$$X_3 = X_1 X_2 \delta_6 \omega_1^3 a\, \ell^3 \csc\varphi \Big/ 8\pi r \rho c_t^4 c_\ell$$

Quantum Mechanical Result

$$X_3 = \left[X_1 X_2 \delta_6 \omega_1^{3/2} \Big/ \rho c c_t^4 (1-a)\right] \sqrt{\pi(ac + \frac{X_1^2}{X_2^2})c_t \ell \csc\varphi \Big/ 8a(a+c)}$$

CASE ⅤA

Classical Theory
Quantum Theory (x $10^2$)

Pyrex

Iron

Displacement Amplitude $|X_3|$

Angstrom Units

Frequency Ratio ($w_2/w_1$)

Pyrex Input:  $X_1 = 20.5$ Å          Iron Input:  $X_1 = 5.77$ Å
              $X_2 = 51.6$ Å                       $X_2 = 15.5$ Å

51
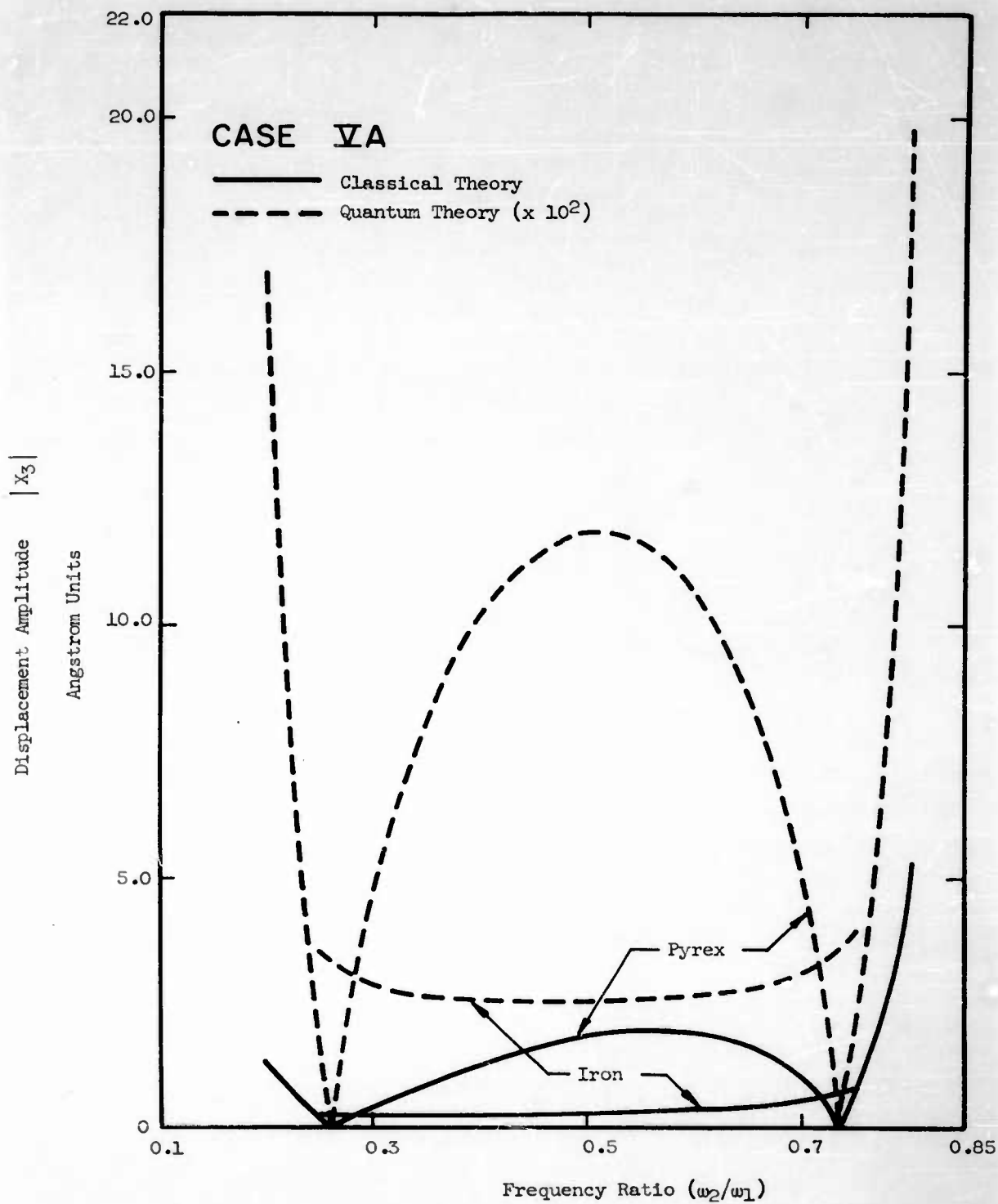
## Case VB

A longitudinal wave interacting with a transverse wave to produce a scattered transverse wave of difference frequency.

$$L(\omega_1) \longrightarrow \qquad\qquad \theta_2 = \theta_3 = 0$$

$$T(\omega_2) \qquad T(\omega_1 - \omega_2)$$
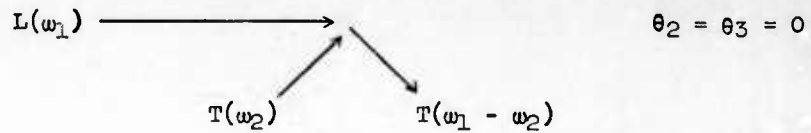
$$\cos \varphi = 1/c + \left[ (c^2 - 1)/2ac \right]$$

$$\tan \varphi = \frac{a \sin \varphi}{c - a \cos \varphi}$$

$$\delta_7 = \left[ (2B + K + A + \frac{7\mu}{3})(c \cos \varphi - a)^2 - (B + \mu + \frac{A}{2})(1 - a)^2 \right]$$

### Classical Result

$$\chi_3 = X_1 X_2 \delta_7 \omega_1^3 a\, \ell^3 \csc \varphi \Big/ 8\pi\rho c_t^4 c_\ell (1-a)$$

### Quantum Mechanical Result

$$X_3 = \left[ X_1 X_2 \delta_7 \omega_1^{3/2} \Big/ \rho c_t^3 c_\ell (1-a)^2 \right] \sqrt{\pi(ac + \frac{X_1^2}{X_2^2})ac_t \ell \csc \varphi \Big/ 8(a+c)}$$

CASE VB

——— Classical Theory

— — — Quantum Theory (x 10$^2$)

Pyrex

Iron

Displacement Amplitude $|X_3|$
Angstrom Units

Frequency Ratio $(\omega_2/\omega_1)$

Pyrex Input: $X_1 = 20.5$ Å        Iron Input: $X_1 = 5.77$ Å
$\quad\quad\quad\quad\quad\; X_2 = 51.6$ Å                    $X_2 = 15.5$ Å

53

# UNCLASSIFIED